Zeolitic imidazolate framework ZIF-67 derived NPC/MoS₂ as efficient supercapacitor electrode material

By

Maryam Raza

Reg. No. 00000330701

Supervised by

Prof. Dr. Naseem Iqbal

US-Pakistan Center for Advanced Studies in Energy (USPCAS-E)

National University of Sciences and Technology (NUST)

H-12, Islamabad 44000, Pakistan

2022

Zeolitic Imidazolate framework ZIF-67 derived NPC/MoS$_2$ as efficient supercapacitor electrode material

By

Maryam Raza

Reg. No. 00000330701

Session 2020-22

Supervised by

Prof. Dr. Naseem Iqbal

A Thesis Submitted to the US-Pakistan Center for Advanced Studies in Energy in partial fulfillment of the requirements for the degree of

MASTER of SCIENCE in

Energy Systems Engineering

US-Pakistan Center for Advanced Studies in Energy (USPCAS-E)

National University of Sciences and Technology (NUST)

H-12, Islamabad 44000, Pakistan

September 2022

THESIS ACCEPTANCE CERTIFICATE

Certified that the final copy of the MS/MPhil thesis written by **Ms. Maryam Raza** (Registration No. 00000330701) of US-Pakistan Center for Advanced Studies in Energy (USPCAS-E), has been vetted by the undersigned, found complete in all respects as per NUST Statues/Regulations, is within the similarity indices limit and is accepted as partial fulfillment for the award of MS degree. It is further certified that necessary amendments, as pointed out by GEC members of the scholar, have also been incorporated in the said thesis.

Signature: _____

Name of Supervisor: _Dr. Naseem Iqbal_
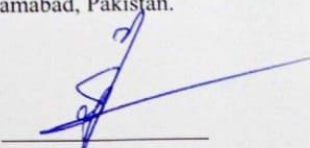
Date: _14/07/2023_

Signature(HOD): _____

Date: _18/7/2023_

Signature (Dean/Principal: _____
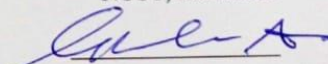
Date: _18/07/2023_

iii

Certificate

This is to certify that work in this thesis has been carried out by **Ms. Maryam Raza** and completed under my supervision in Synthesis and Energy Storage laboratory, US-Pakistan Center for Advanced Studies in Energy (USPCAS-E), National University of Sciences and Technology, H-12, Islamabad, Pakistan.
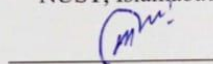
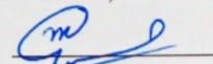Supervisor: _____
Prof. Dr. Naseem Iqbal
USPCAS-E
NUST, Islamabad

GEC member 1: _____
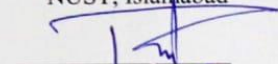Dr. Ghulam Ali
USPCAS-E
NUST, Islamabad

GEC member 2: _____
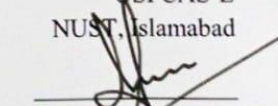Dr. Nadia Shahzad
USPCAS-E
NUST, Islamabad

GEC member 3: _____
Dr. Mustafa Anwar
USPCAS-E
NUST, Islamabad

HOD-ESE: _____
Dr. Rabia Liaquat
USPCAS-E
NUST, Islamabad

Dean/Principal: _____
Prof. Dr. Adeel Waqas
USPCAS-E
NUST, Islamabad

Dedication

To my parents, who supported me in every aspect of life, my siblings and friends

Acknowledgments

All praise be to Allah Almighty, who has bestowed me the opportunity to pursue knowledge and enabled me to fulfill my obligation to explore the field of science possible up to my maximum limits. Indeed, without YOUR blessings, this mammoth task would not have been possible. And I acknowledge that without YOUR willingness and guidance, I would not have done a single task. I am grateful to my parents for their unconditional love and sacrifices. your debt for your encouragement, financial and moral support. Thank you for keeping confidence in me.

I want to express my sincere gratitude to **Prof. Dr. Naseem Iqbal**, my research supervisor, for his motivation, continuous support, patience, and immense knowledge. He has been my total guide throughout my studies. Working under his supervision has enlarged my horizons. I am thankful to my GEC members**, Dr. Ghulam Ali, Dr. Nadia Shahzad, and Dr. Mustafa Anwar**, for sparing precious time from their busy schedules and for suggestions and moral support. I also want to thank the USPCASE faculty for being extremely cooperative.

A special thanks to lab engineers at the Synthesis lab, AEMS lab, and Combined lab Muhammad Naveed Ahmad, Aamir Satti, and Nisar Ahmad, who helped me greatly in the experimental work and testing.

Last but not least, I would pay my regards to my family for their unparallel love, support, and encouragement throughout my research work and to my friends and lab fellows Iqra Shaukat, Rabbia Naz, Rabia Ahmad, Rimsha Mehek, Neelam Zaman, accompanied me in this journey.

Maryam Raza

Abstract

In this study, I aimed to synthesize a composite material by combining ZIF-67 (Co) and molybdenum disulfide (MoS_2). ZIF-67 is a type of zeolitic imidazole framework, which was first synthesized and annealed in a reducing environment consisting of a mixture of argon and hydrogen gases. I added different amounts of annealed ZIF-67/NPC (nanoparticles) during the hydrothermal preparation of MoS_2, keeping the amounts of Mo and S constant. I prepared three samples with different molar ratios of Mo to Co: $Mo_1:Co_{0.5}$, $Mo_1:Co_1$, and $Mo_1:Co_2$.

X-ray diffraction (XRD) analysis was performed to confirm the formation of a MoS_2/Co_3S_4 composite. The incorporation of Co/NPC significantly improved the electrochemical properties of MoS_2. The specific capacitance of the samples was measured using electrochemical measurements, and found that the sample with equal masses of Mo and Co/NPC had a high specific capacitance of 612 F g^{-1}. This indicated that the composite material had a high capacity to store electrical charge.

Furthermore, the cyclic stability of the composite material was tested by subjecting it to 9000 cycles of charge and discharge. The material showed a high cyclic stability of 88.59%, indicating that it was durable and could maintain its electrochemical properties even after prolonged use. Among the three samples, the $Mo_1:Co_1$/CMS-2 sample showed the best performance, with the highest specific capacitance and cyclic stability. This result suggested that the $Mo_1:Co_1$ ratio was the optimum ratio for synthesizing the composite material. Overall, this study demonstrated the potential of ZIF-67-based MoS_2 composites for use in energy storage applications.

Keywords: Molybdenum Sulphide, Cobalt Sulphide, Supercapacitor, ZIF-67, Pyrolysis, Specific Capacitance.

Table of Contents

List of Figures

List of Tables

List of Publication

Journal: Zeolitic imidazolate framework ZIF-67 derived NPC/MoS$_2$ as efficient supercapacitor electrode material

Status: Submitted in Journal of Electroanalytical Chemsitry

List of Abbreviations

SCs	Supercapacitors
EDLC	Electric double layer capacitance
C	Carbon
2mim	2-methyle imidazole
GO	Graphene oxide
rGO	Reduced graphene oxide
ZIF	Zeolitic imidazole framework
MOF	Metal organic framework
NGC	Nanographitic carbon
MOs	Metal oxides
CNT	Carbon nanotubes
Li-ion	Lithium ion
XRD	X ray Diffraction
TGA	Thermogravimetric analysis
SEM	Scanning Electron Microscopy
EIS	Electrochemical impedance spectroscopy
CV	Cyclic voltammetry
CP	Chronopotentiometry
GCD	Galvanic Charge Discharge
C	Capacitance
m	Mass loading
FTIR	Fourier transform infrared spectroscopy
EDS	Energy dispersive X-ray spectroscopy
V	Voltage

Chapter 1: Introduction

1.1 Background

Most of the electrical energy used in the world today comes from fossil fuels. As a result, several businesses have created new regulations to aid in lowering CO_2 emissions and halting global warming. Due to this, the vehicle sector has emerged as a key area of analysis for determining how using fossil fuels affects the environment. The energy sector struggles to keep up with the population's continued growth to provide the world's ever-growing need for energy. As a result, it has been suggested that using renewable energy sources is a practical way to achieve the goal of increasing energy efficiency. With such wide variations in electrical generation, solar and wind energy technologies are becoming practical possibilities.[1]

To combat climate change, air pollution, and a depleting fossil fuel supply, renewable resources are currently being investigated. To protect the environment and replace fossil fuels, it is more important than ever to have access to green energy-generating and functioning energy storage technologies. Supercapacitors and batteries have grown significantly in importance as a result of the enormous progress made in the production of renewable solar and wind energy. Batteries and supercapacitors are becoming increasingly crucial as the use of hybrid and electric vehicles, which produce almost no CO_2, grows.[2] Supercapacitors have received a lot of interest recently due to their high power density and cycle life of more than 100,000 cycles. They have also been shown to have a better power density than standard capacitors and a higher energy density compared to batteries. Their characteristics influence the performance of supercapacitors critical for energy storage devices to maximize material. Because of this, the energy research team is still developing effective intermediate hybrid materials that combine the traits of both types of energy storage.[3] For instance, carbon-based materials are essential in developing clean and sustainable energy technologies like batteries, supercapacitors, and fuel cells because of their high electrical conductivity, large specific surface area, chemical and thermal stability, and low cost. Supercapacitors, used in hybrid systems to generate high power that a lithium battery cannot offer reversibly, use carbon. The electrodes are large-surfaced carbon nanostructures. New carbon compounds with regulated nanostructure and surface activity are required for increased storage

1

capacity and cycle ability. Supercapacitors have a simple operating principle and quick charge-discharge rates. The Ragone plot, shown in Figure 1.1, shows the relationship between power density and energy density for the most important energy storage methods. In terms of particular energy and specific power, supercapacitors play a large role in the story and are an important plot point.[4] They are the best option to meet the rising needs of energy storage devices since they provide a higher power density (better than lithium batteries and a better energy density) (superior to standard capacitors). Supercapacitors are used in various applications, including consumer electronics, memory backup systems, industrial power, energy management, and equipment for military and public transportation. Their installation has recently demonstrated supercapacitors' reliability and safety in the emergency escape doors of A380 aircraft.[3]

Ordinary dielectric capacitors often have greater energy densities (5–10 Wh/kg), but supercapacitors typically have lower densities. For instance, a typical lithium-ion battery has a specific energy of 120–170 Wh/kg. Nevertheless, for continuous energy provision over extended durations, a combination of batteries (or any other energy source) is needed. More work has to be done before supercapacitors can match or even surpass batteries in terms of energy performance.
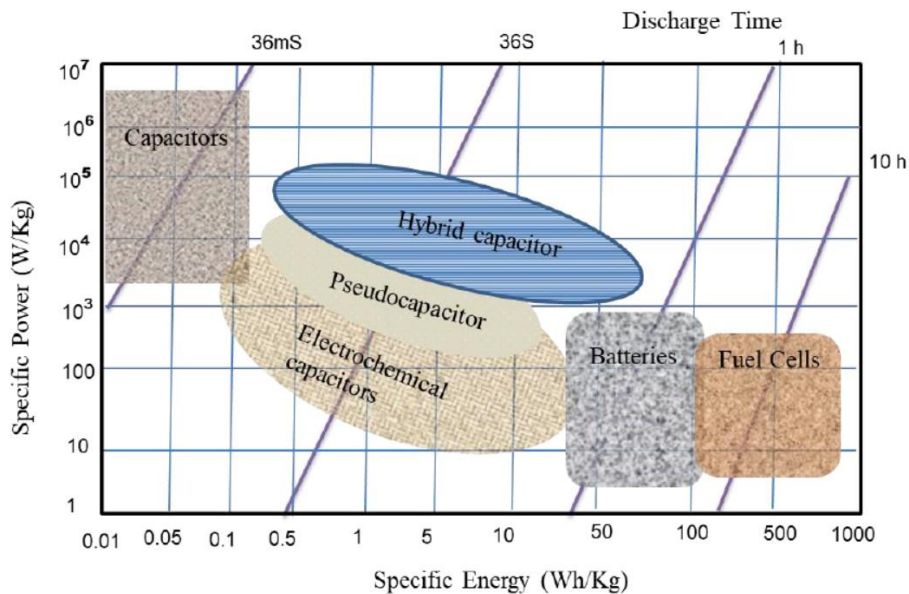
Figure 1.1 Energy and power related to conventional energy storage and conversion technologies.[5]

Whereas batteries and fuel cells have a high power density (about 106 W/kg), standard supercapacitors have a modest power density (around 106 W/kg). The energy density of

2

supercapacitors is higher than that of traditional capacitors. Supercapacitors store charge in an electric double layer, also known as an electric double layer, created by ions at the interface of the active surface area of carbon and the electrolyte.[6]

1.1.1   EDLC Super-capacitor

The pure electrostatic charge collected at the electrode/electrolyte interface serves as the source of capacitance in electrical double-layer capacitors (EDLCs). The most well-known materials that exhibit EDLC activity are those based on carbon. The electrolyte's ions have easy access to their enormous surface area. A typical EDLC may be maintained for millions of cycles with a specific energy of 5 Wh/kg. The physical state of the electrodes does not change when charging or discharging.[1]

1.1.2 Pseudocapacitors

Pseudocapacitors employ quick faradic redox reactions. Electrically conducting polymers, transition metal oxides, transition metal sulfides, and transition metal nitrides are the most frequently utilized electrode materials in pseudocapacitors. This fictitious capacitance can be placed on top of an electric double-layer capacitance. Compared to EDLCs, their specific energy is superior. Owing to intrinsic chemical changes in electrodes brought on by faradic reactions, they have a low specific power and a limited lifespan. Both procedures can potentially have a collaborative influence and can occur simultaneously. Yet, the kind of electrode material is essential for it to happen.[7]

1.2 Comparison between batteries and supercapacitors

Batteries that can be recharged electrochemically store energy. Rechargeable batteries that are available commercially provide a variety of possibilities, including lithium batteries [8]. Moreover, batteries take longer to charge and discharge than supercapacitors do due to slower chemical processes, which affects their power/energy density (see Figure 1.2) and leads to longer charge and discharge times. Supercapacitors self-discharge noticeably quicker than batteries, which can hold a charge and maintain voltage for longer[8]. Supercapacitors have a lower energy density than Li-ion batteries because of their low internal resistance but can provide 10 times as much power.

Figure 1.2 The supercapacitor vs. battery.[9]

Besides having a long cycle life, supercapacitors can discharge and charge quickly. Further benefits include using low-cost materials, basic construction concepts, and building techniques. Supercapacitors give cutting-edge charge indication ($Q = f(V)$) and can be used in hybrid applications with rechargeable batteries. Nevertheless, they are limited to low-voltage operation[9].

1.3 Supercapacitor: Charge storage mechanism and operating principle

An ultra-capacitor with two conducting electrodes and dielectric insulation is depicted in Figure 1.3. The electrode-to-electrolyte contact. Figure 1.4 shows where the charging accumulator is located in the two-plate EDLC capacitor. Via the outer loop, electrons are moved from the negative to the positive electrodes during charging. Charges are generated and transferred between the two layers due to the redox process that occurs on the electrode. The power density of EDLC may be lower than that of pseudocapacitors due to the lower power density of Faradaic systems.[2, 11] Pseudo-capacities frequently have higher specific capacities and energy densities than EDLC since they are a Faradaic device.
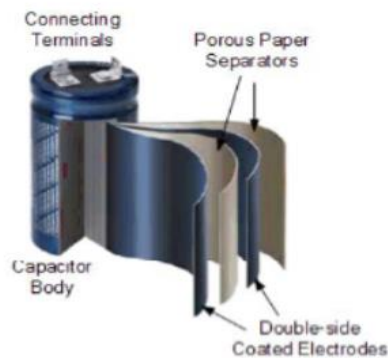
Figure 1.3 Supercapacitor construction[11]

Figure 1. 4 shows how the capacitor is charged with voltage, which causes opposing charges to accumulate on each electrode and produces an eclectic field that enables the capacitor to store energy. A system's capacitance, C, may be expressed as:

$$C=Q/V \qquad (1)$$

V represents for the applied voltage, while Q stands for the stored charges. The electrode surface area A determines the capacitance C, which is inversely proportional to the electrode distance. Thus, capacitance may be described as

$$C=\mathcal{E}_{o}\,\mathcal{E}rQ/V \qquad (2)$$

Between the electrodes, εr acts as an isolating material, while εo, the dielectric constant, always has a relative permittivity. The energy and power density of a supercapacitor are used to calculate its output using Eqs. (1) and (2).
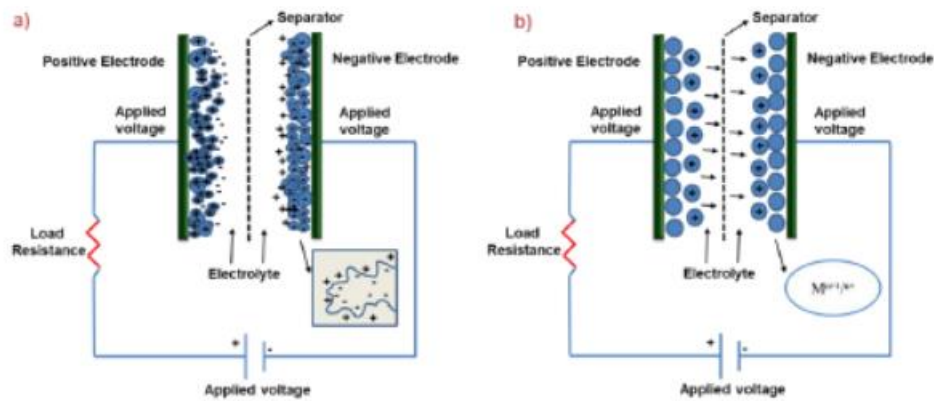
Figure 1.4 Supercapacitors Schematic Diagram. (A) EDLC; (B) pseudo-capacitor (M stands for the metal atom)[12]

Using supercapacitor charge processing, power density rises. EDLs produce electrostatic interactions at electrode/electrolyte interfaces. Capacitance is based on the charge present on the electrode surface. . Early anchoring cations create a tightly packed Helmholtz layer (IHL). Second, anions are drawn towards the IHL ions in the outer Helmholtz layer (OHL). The size, concentration, surface charge density, and other characteristics of the ions all impact the capacitance of the electrical double layer[13].Figure 1.6 illustrates the division of the pseudo-capacitive reactions into three categories. "Under-potential deposition" is the term for the electrodeposition of a material at a lower voltage than the reduction potential in theory.
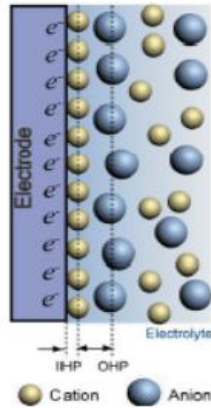
Figure 1.5 Schematic EDL Structure [12]

The testimony of thin lead films on gold substrates is a classic example. One example of this is thin lead (Pb) films on gold substrates (Au)[14].

For these reasons, the near-surface redox reaction is the pseudo capacitive reaction that is most commonly seen. Some pseudo-capacitive materials, like ruthenium dioxide, have active spots that may store electrons due to redox activities (e.g., electron transfer reactions). Quick ion insertion-desertion is an example of a pseudo-capacitive process. Reactions of this kind include both batteries and capacitive ones. The sole distinction between them is if phase transitions occur[15].
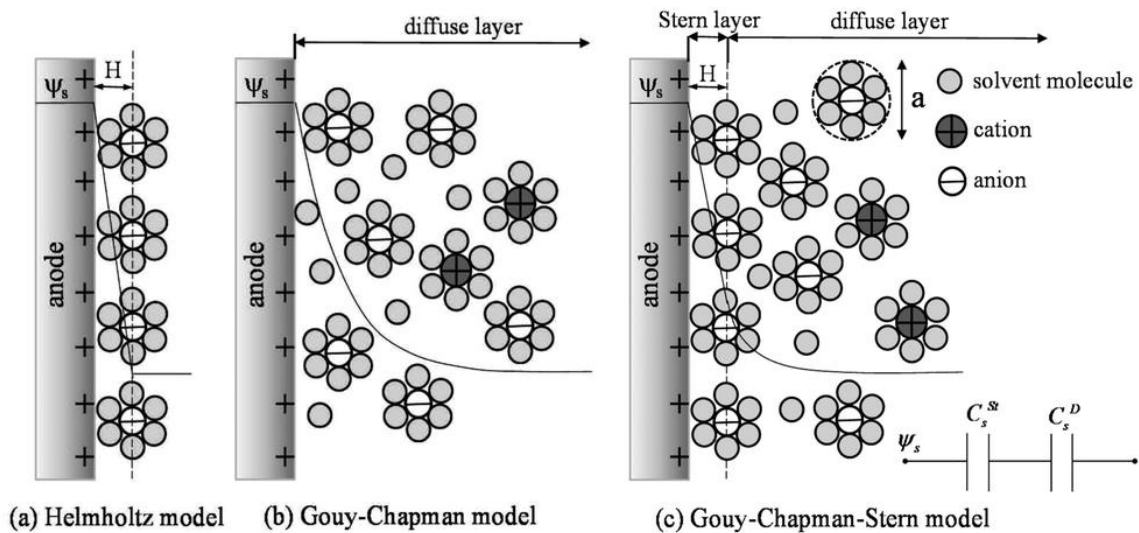
Figure 1.6 (a) Helmholtz Model (b) Gouy-Chapman Model (c)Stern model [13].

1.4 Supercapacitors Evaluation

The supercapacitor resembles a battery in terms of construction. In a single-cell supercapacitor, both electrodes interact with an electrolyte solution that is split by an insulator, as seen in Figure 1.7. [16]The cell's components are all comparable to two straightforward capacitors connected in series. The equivalent resistor and capacitor (RC) circuit for a single supercapacitor. Anodic and cathodic capacitances are denoted by Ca and Cc, respectively. the cellular equivalent series resistance is represented by the quantity Rs (ESR). RF is a single electrode's self-discharge resistance. To get the total capacitance (CT) of the complete cell, equation (3) is used. Because the total capacitance (CT) in this instance is equal to half of the capacitance of any single electrode, the supercapacitor is shown to be symmetric[17].

$$\frac{1}{C_T} = \frac{1}{C_a} + \frac{1}{C_c} \tag{3}$$
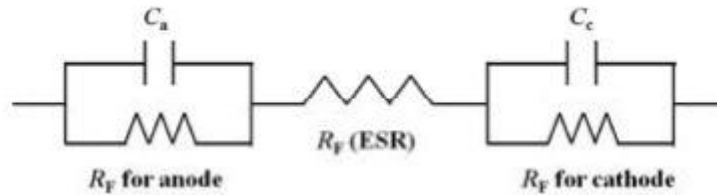
Figure 1.7 Resistor-capacitor (RC) equivalent circuit for supercapacitor[17]

Ca is not equal to Cc when the materials of the two electrodes differ; this asymmetric supercapacitor is then described (ASC). CT is dominated by one with a smaller capacitance. Overall, capacitance and stored charge are significantly influenced by the electrode material. Equations (4) and (5) may be used to express E as the energy stored and P as the specific power for a single-cell supercapacitor (5) [18] .

$$E = \frac{1}{2}C_T V^2 \tag{4}$$

$$P = \frac{V^2}{4R_s} \tag{5}$$

Where the cell voltage (V), the cell capacitance (F), and the electrode surface resistance (ESR) (ohms). The following equations make it clear that V, CT, and Rs are important restrictions to be mindful of for the super-capacitor's ultimate performance. The cell's voltage is a function of the

electrode materials and the thermodynamic stability of the electrolyte solution. The inherent electronic characteristics of the electrolyte solution and electrode matrix, as well as the mass transfer resistance of the ions and the interaction resistance between the electrode and the current collecting plate, all affect the electric field strength (ESR)[19]. To optimize the capacity of the whole cell, the capacitance of both electrodes must be increased. A supercapacitor has to have a high capacitance value, a high working cell voltage, and a low ESR in order to function properly. To improve the overall performance of supercapacitors, additional research and development are required to create new better electrode materials[20].

Figure 1.6 depicts a three-electrode electrochemical cell (beaker cell). The electrochemical performance of a material is evaluated on a lab scale using a beaker cell. The substance being evaluated for performance is on the working electrode of the beaker cell. an electrode used as a reference to which potential may be applied and measured. Counter electrodes help with potential application and finish the circuit so that current may flow. From a three-electrode cell design, the specific capacitance of a single electrode is computed[21].
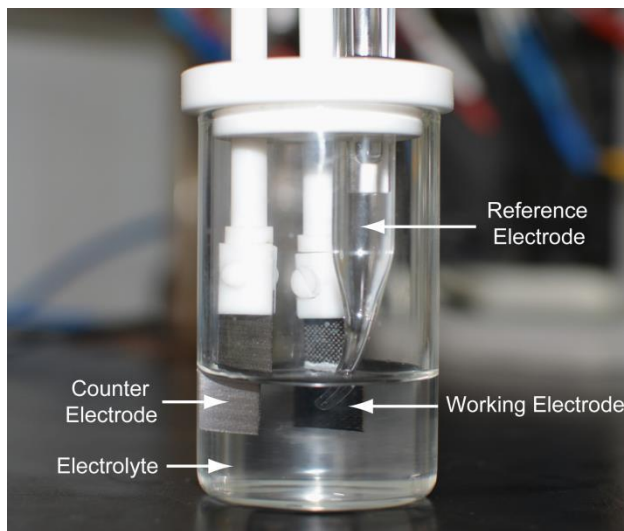
Figure 1.8 A three-electrode Beaker cell [21]

The electrochemical activity may be evaluated more precisely since the performance of a two-electrode test fixture closely resembles that of a packed supercapacitor cell. These may be manufactured from two stainless steel plates or bought commercially. A two-electrode

arrangement allows for the examination of both electrodes individually, whereas a three-electrode cell only allows for the investigation of the working electrode[22].

It is significant to note that in the three-electrode cell, the applied potential on the working electrode is completely applied to the working electrode and is determined by the reference electrode that is being utilized. Every electrode in a two-electrode cell receives an equal share of the electric potential supplied to the system. As a result, the working electrode in a three-electrode cell experiences a potential range twice as large as that of a two-electrode cell, leading to a computation of capacitance that is twofold. When the RE and WE are close together in two-electrode cells, the RE can precisely regulate the interfacial potential. Supercapacitor performance is assessed at the packed cell level using these characteristics[21].

1.5 Application of Supercapacitors

1.5.1 Industrial applications

Supercapacitors cannot store or deliver as much energy as conventional capacitors and batteries. Supercapacitors are also suited for various applications in the industry due to their rapid charge and discharge rate and prolonged cycle life[23].

1.4.2 Backup power sources

Consumer supercapacitors are frequently used as backup power for clocks, system boards, and microcomputers. In the event that the main power source is cut off or malfunctions, these devices provide electricity. You may record preset radio stations or taxi rates using the in-car audio system and taxi meter[24].

1.5.3 Main power sources

From a supercapacitor, one or more large pulses (mss) may be supplied. They must act as the main power source in the system's architecture for several frequent purposes. For instance, a battery or a wall charger might be used to recharge the supercapacitor in a toy car.

1.5.4 Alternate power sources

In addition to batteries, there were a number of alternative power sources available for the following purposes: The solar watch can be used for several days thanks to the supercapacitor that the solar panel has charged. Road marking lights and traffic signs are powered by solar cells and supercapacitors.

1.5.5 Vehicles applications

Supercapacitors are excellent at storing large amounts of energy for a brief period. These batteries are used to store regenerative braking energy. This energy is used in the following stage of the acceleration process. In this case, supercapacitors could assist in minimising the size of the primary power source.

1.5.6 Industrial process

Supercapacitors could provide a more consistent power source and a better energy-to-weight ratio. Power outages and other voltage changes might affect some industrial activities. If the power source is cut off, there will be a significant loss of production.

1.6 Problem Statement

Although much effort has been made to create high-performance energy storage devices using various electrode materials and liquid electrolytes, these devices are unreliable and only store a small amount of energy. For applications like electronic devices and electric vehicles, devices with higher energy and power densities are required. Greater power densities and faster charge-discharge rates are only a few advantages supercapacitors have over batteries. The primary issues in commercializing supercapacitors are their low energy density (caused by their low active material content) and poor cycle stability (which causes structural deterioration over prolonged cycling durations). The major difficulty is maintaining power density and safety while increasing energy density. This problem requires the increased energy density of supercapacitors with high ionic and electronic conductivity and a safe operating voltage.

1.7 Objectives

Finding suitable electrode materials, such as ZIF-derived nonporous carbon-based oxides and sulfides with characteristic structures and porous textures, is the main goal of this research. In other words, the ZIF offers a unique approach to synthesizing two materials from a single precursor: nitrogen-doped porous carbon and metallic particles embedded in a carbon matrix produced from ligands.

• Low-cost materials are used to synthesize nonporous carbon-based electrode materials generated from ZIF.

• Research the impact of pyrolised ZIF-67 on the electrode structure

References

[1]   M. Jayalakshmi and K. Balasubramanian, "Simple capacitors to supercapacitors-an overview," *Int. J. Electrochem. Sci,* vol. 3, no. 11, pp. 1196-1217, 2008.

[2]   Y. Shao *et al.*, "Design and mechanisms of asymmetric supercapacitors," *Chemical reviews,* vol. 118, no. 18, pp. 9233-9280, 2018.

[3]   A. G. Pandolfo and A. F. Hollenkamp, "Carbon properties and their role in supercapacitors," *Journal of power sources,* vol. 157, no. 1, pp. 11-27, 2006.

[4]   S. Satpathy, S. Das, and B. K. Bhattacharyya, "How and where to use super-capacitors effectively, an integration of review of past and new characterization works on super-capacitors," *Journal of Energy Storage,* vol. 27, p. 101044, 2020.

[5]   M. Lu, *Supercapacitors: materials, systems, and applications*. John Wiley & Sons, 2013.

[6]   M. S. Halper and J. C. Ellenbogen, "Supercapacitors: A brief overview," *The MITRE Corporation, McLean, Virginia, USA,* vol. 1, 2006.

[7]   Y. Wang, Y. Song, and Y. Xia, "Electrochemical capacitors: mechanism, materials, systems, characterization and applications," *Chemical Society Reviews,* vol. 45, no. 21, pp. 5925-5950, 2016.

[8]   S. Cheng *et al.*, "Phase evolution of an alpha MnO2-based electrode for pseudo-capacitors probed by in operando Raman spectroscopy," *Nano Energy,* vol. 9, pp. 161-167, 2014.

[9]   P. Simon and Y. Gogotsi, "Materials for electrochemical capacitors," *Nature materials,* vol. 7, no. 11, pp. 845-854, 2008.

[10]   M. Salanne *et al.*, "Efficient storage mechanisms for building better supercapacitors," *Nature Energy,* vol. 1, no. 6, pp. 1-10, 2016.

[11]   Y. Wang and Y. Xia, "Recent progress in supercapacitors: from materials design to system construction," *Advanced materials,* vol. 25, no. 37, pp. 5336-5342, 2013.

[12]   Z. Wu, L. Li, J. m. Yan, and X. b. Zhang, "Materials design and system construction for conventional and new-concept supercapacitors," *Advanced science,* vol. 4, no. 6, p. 1600382, 2017.

[13]   Z. Li, J. Lin, B. Li, C. Yu, H. Wang, and Q. Li, "Construction of heteroatom-doped and three-dimensional graphene materials for the applications in supercapacitors: A review," *Journal of energy storage,* vol. 44, p. 103437, 2021.

[14] X. Yu, B. Lu, and Z. Xu, "Super long-life supercapacitors based on the construction of nanohoneycomb-like strongly coupled CoMoO4–3D graphene hybrid electrodes," *Advanced materials,* vol. 26, no. 7, pp. 1044-1051, 2014.

[15] J. F. Snyder, D. J. O'Brien, D. M. Baechle, D. E. Mattson, and E. D. Wetzel, *Structural composite capacitors, supercapacitors, and batteries for US Army Applications*. 2008.

[16] J. Chae, K. Ng, and G. Chen, "Nanostructured materials for the construction of asymmetrical supercapacitors," *Proceedings of the Institution of Mechanical Engineers, Part A: Journal of Power and Energy,* vol. 224, no. 4, pp. 479-503, 2010.

[17] W. Lu, J. Shen, P. Zhang, Y. Zhong, Y. Hu, and X. W. Lou, "Construction of CoO/Co-Cu-S hierarchical tubular heterostructures for hybrid supercapacitors," *Angewandte Chemie,* vol. 131, no. 43, pp. 15587-15593, 2019.

[18] H. Li *et al.*, "Quantifying the volumetric performance metrics of supercapacitors," *Advanced Energy Materials,* vol. 9, no. 21, p. 1900079, 2019.

[19] C. Liu, Q. Li, and K. Wang, "State-of-charge estimation and remaining useful life prediction of supercapacitors," *Renewable and Sustainable Energy Reviews,* vol. 150, p. 111408, 2021.

[20] M. Z. Iqbal, M. M. Faisal, and S. R. Ali, "Integration of supercapacitors and batteries towards high-performance hybrid energy storage devices," *International Journal of Energy Research,* vol. 45, no. 2, pp. 1449-1479, 2021.

[21] A. Allagui, A. S. Elwakil, B. J. Maundy, and T. J. Freeborn, "Spectral capacitance of series and parallel combinations of supercapacitors," *ChemElectroChem,* vol. 3, no. 9, pp. 1429-1436, 2016.

[22] L. Sun *et al.*, "Nitrogen-doped porous graphitic carbon as an excellent electrode material for advanced supercapacitors," *Chemistry–a european journal,* vol. 20, no. 2, pp. 564-574, 2014.

[23] H. Gualous, H. Louahlia-Gualous, R. Gallay, and A. Miraoui, "Supercapacitor thermal modeling and characterization in transient state for industrial applications," *IEEE Transactions on industry applications,* vol. 45, no. 3, pp. 1035-1044, 2009.

[24] Y. Zhan, Y. Guo, J. Zhu, and L. Li, "Power and energy management of grid/PEMFC/battery/supercapacitor hybrid power sources for UPS applications," *International Journal of Electrical Power & Energy Systems,* vol. 67, pp. 59

Chapter 2: Literature Review

2.1 Electrode materials for supercapacitors

In a patent application submitted in 1957, Backer proposed a basic supercapacitor concept. When he built the supercapacitors, he used a carbon electrode with a lot of surface area and an electrolyte made of aqueous H2SO$_4$.[1]The electrodes, electrolytes, and separators are the three main components of a supercapacitor. The electrodes are a crucial component in charge/discharge transport and were utilized to calculate a supercapacitor's energy and power densities. The material of the supercapacitor's electrode has a significant impact on its electrochemical performance. As a result, selecting an efficient and effective electrode material for a high-performance supercapacitor is critical. Nanostructure and nanocomposite are two of the most common approaches (Figure 2.1). To build a supercapacitor, the electrodes must have a high surface area and be made of porous carbon. Diffusion via the electrolyte transports the migrated ions to produce the double layers between the electrodes [2]. Higher energy densities are achieved using transition metal oxides and electroactive polymers, but each has constraints.
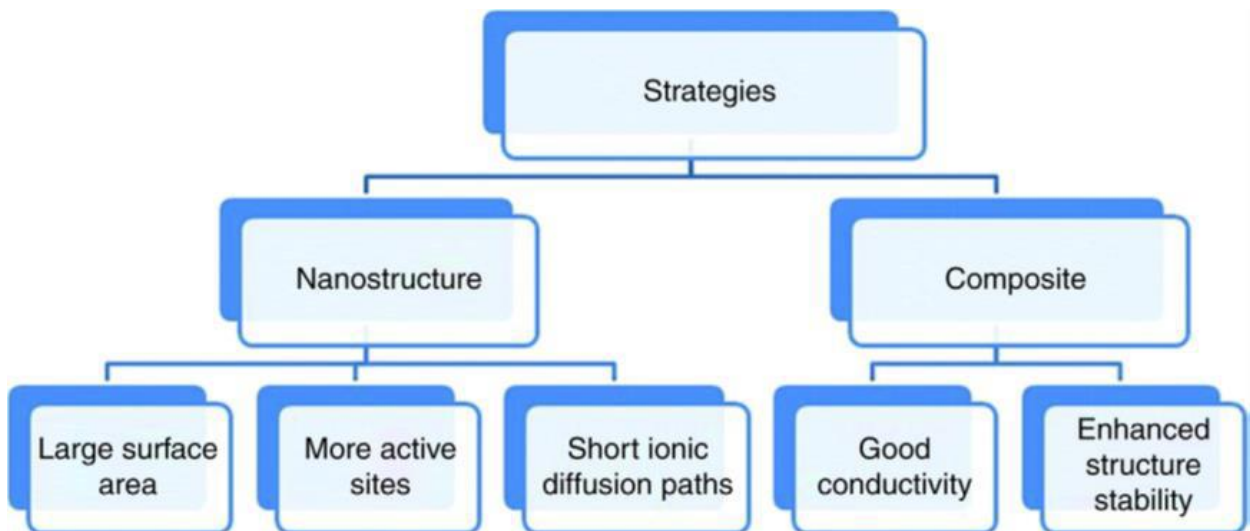
Figure 2.1 Strategies to enhance the performance of supercapacitors [3].

The first has a significant cost problem, while the second has stability [3]. There are three classes of pore sizes distinguished within the electrode material. The micropores have a width of less than 2 nm and are the tiniest. Mesoporous are pores with a diameter of 2 to 50 nm [4]. Activated carbon electrode materials have several limitations, and a better electrode material must address these shortcomings and have a higher surface area, mesoporosity, electrical conductivity, and electrolyte access. CNTs have been considered materials for supercapacitor electrodes to develop storage energy [5].

2.2 Recent Electrode Materials for Supercapacitors

The electrode material employed in a supercapacitor may also impact its electrochemical performance. In contrast to the ideal, most electrode materials excel only in one of these aspects. Choosing electrode materials for both types of storage is shown in Figure 2. 3, using the same criteria and procedures. As previously noted, the electrode materials of a supercapacitor have a substantial influence on the device's capacitance and charge storage capabilities [6]. As a result, they are developing new materials with more capacity and functionality than present electrode materials, which is a highly effective approach to addressing issues. The high surface areas of the electrode materials have a significant impact on supercapacitor capacitance. A material's capacitance cannot be directly related to its surface area, as all its surface area is not accessible when it encounters an electrolyte. A more precise definition of the electrochemically active surface area may be more accurate when addressing the capacitance of electrodes on surfaces. The electrode material's pore size is critical to its ability to conduct electricity [7]

As shown in Equation (1), a pore's capacity is reduced because the average distance between an ion and its pore wall rises. High-capacity manufacturing's porosity measure comprises the pore size and distribution of pore sizes in a certain material area. Capacitive capacity depends heavily on the electrode surface area that electrolytes can access. Metal oxide-based supercapacitors are characterized by their long-running periods and high specific capacitance [5]. The most significant downside to this material is its very high cost. Conducting polymers can hold redox and have a large surface area for conducting electricity, making them excellent conductors [7]. Carbon is the most utilized electrode material in supercapacitors. In recent years, carbon-based supercapacitors have risen in prominence. The performance of supercapacitors may be improved by creating porous nanostructures with more charge transfer active sites and ion adsorption. There are three

basic types of electrode materials: Metal oxides, carbon compounds, and conductive polymers are all examples of transition metal-oxides [5-8]. When it comes to carbon-based material carbonaceous chemicals increase the interaction of deposited material and electrolyte and, thus, consequently, the conductivity [8]. The active surface area usually is low, and the pore size distribution is also challenging to tailor due to the rigid morphology of metal oxide-based electrodes. Porous nanostructures with more ion adsorption and charge transfer active spots may improve efficiency [9]. CNTs have unique features that make them ideal for supercapacitors. Polymer coordination polymers (PCPs) are one of the various metal-organic compounds that may be classified into three-dimensional or multi-dimensional structures [9-10]. Because they act as both sacrificial templates and metal precursors, MOFs are very useful. These materials may help build nano, micro, and hollow-structured materials with functional shells [11]. These porous materials have received much attention because of their increased surface area, adjustable pores, and flexible architectures. Several research groups work together to create MOF materials at the nano and microscale. Elsevier and other respectable publications have also published various research articles focusing on MOFs. Using MOFs as a template for functional nanostructures is also discussed [12].

2.2.1 Zeolitic-Imidazolate framework (ZIF) based electrodes

By mixing organic and inorganic ingredients, zeolitic imidazolate frames (ZIFs) may be manufactured with various properties such as unique particle morphologies, excellent porosity, and surface functionality [13]. ZIFs can be converted to nanoporous carbon (NPCs) or metal Compounds Different morphologies via selective pyrolysis in a controlled environment may be transformed, as demonstrated in Figure 2. 2. Changes to the surfaces of composites made up of organic and inorganic parts, the volumes of pore structures, and the surface areas of the composites could lead to the creation of parent ZIFs. The porous nature of ZIFs is being investigated as a template used for porous carbon and metal-oxides due to their porous nature. These materials have small diffusion routes and increased pores on their surface area, allowing interfacial and electrolyte transport [12-14]. Because of their inherent variability, ZIF-derived carbons outperform conventional carbon-based materials using standard processes, templates, or precursors. Over the last decade, ZIF-derived materials have been extensively used in the electrochemical conversion and energy storage

17
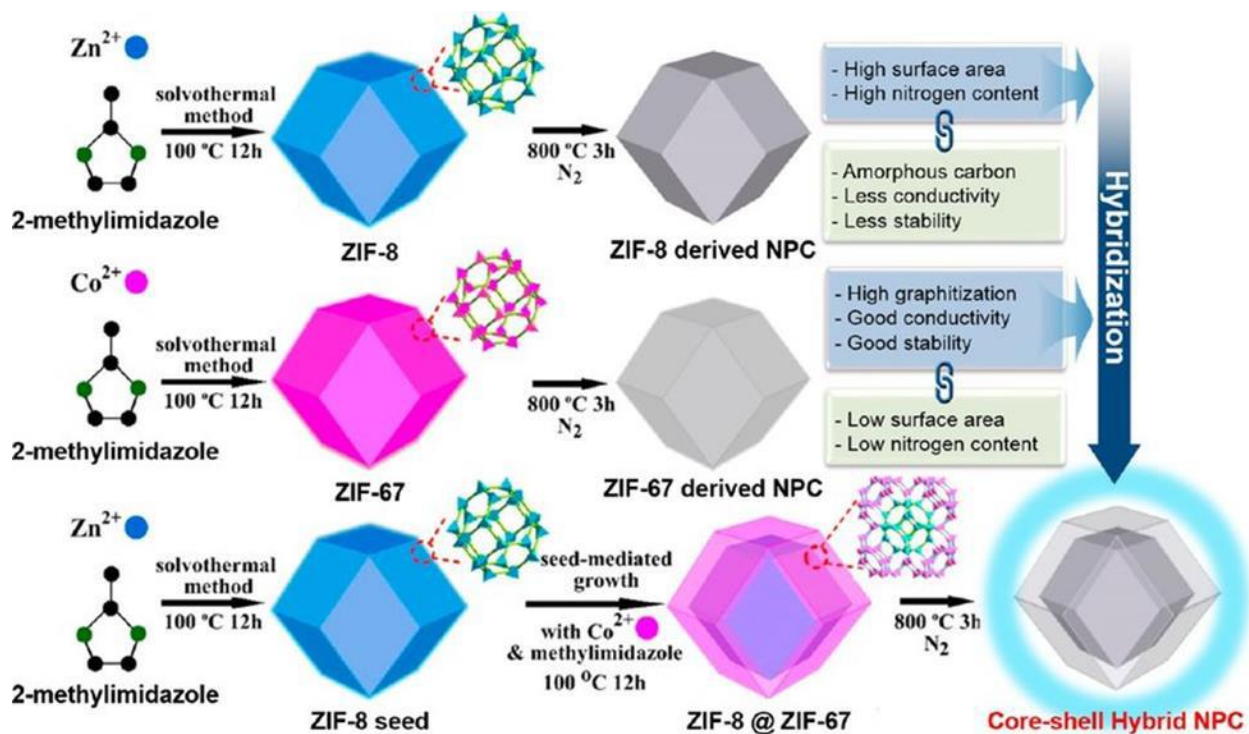
Figure 2.2 Synthesis schemes of nanoporous carbon derived from ZIF-8 and ZIF-67 [13].

2.2.2 Nanoporous Carbon (NPC) derived from ZIFs

Achieving ZIF materials' desired characteristics and morphologies involves carefully selecting starting materials and synthesis conditions [14]. Solvothermal, sono chemical, and hydrothermal processes are a few of the many synthesized ones that have been developed to date [15]. On the other hand, porous carbon-based ZIFs are synthesized from powder ZIFs (see Figure 2. 3). Various solvents are often used in the solvothermal synthesis process. Depending on the precursors employed, this reaction might take several hours to complete [16]. An ambient environment was used to mix the cobalt and 2-methyl imidazole solutions, afterwards, the precipitates were thoroughly washed and then dried in the oven. A controlled two-step annealing cycle in a reducing environment (Ar/H$_2$) may be employed further to convert ZIF-67 into carbon nanotubes [17]. The hydrothermal approach for synthesizing ZIFs, which uses water as a solvent, has grown more popular recently.
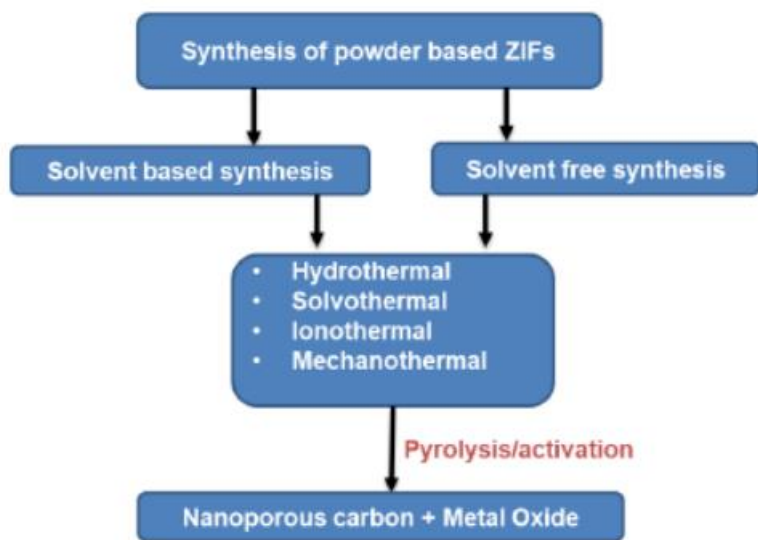
Figure 2.3 Summarized the synthetic method for ZIFs to ZIF-derived nano-porous carbon and metal oxide [18].

To facilitate the facile synthesis of organic-inorganic ZIF networks, several metal ZIFs may be employed, and altering the reaction conditions, temperature, and duration can result in the formation of various ZIF coordination structures [19-20]. To fabricate ZIF-67, a mixture of cobalt nitrate hexahydrate and 2-methyl imidazole was stirred at room temperature, and the resulting precipitate was then cleaned and vacuum-dried. Utilizing a controlled two-step annealing cycle in an Ar/H$_2$ atmosphere, carbon nanotubes can be produced from ZIF-67. Figure 2.4a depicts the bimetallic ZIF crystal structure, which undergoes a color change from white to purple, lavender, and eventually purple, depending on the cobalt ratio in the composition (Figure 2.4b). The ZIF powders exhibit a polyhedral morphology (Figure 2.4c) according to the data [19] [17]. Co3O4 hollow nanostructures with rhombic dodecahedral nanostructures were produced by Huang and colleagues using ZIF-67 as a precursor and a two-step calcination process [20]. The sol-gel technique is one of the simplest methods for producing materials with greater concentration and uniformity. The sol-gel technique (gel) generates a grid of interconnected microparticles via solution agglomeration under specific conditions. The sol-gel process employs colloidal, alkoxide, or polymeric precursors, which can be classified into two categories: alkoxide and colloidal. NiCo$_2$O$_4$ thin films were deposited using a sol-gel process by Liu and colleagues [21], who reported improved specific capacitance of 2157 F/g and high cyclic stability (96.5%) over 10,000

cycles. As shown in Figure 2, a hybrid ZIF may be synthesized from metal precursors and organic linkers to produce porous carbon.
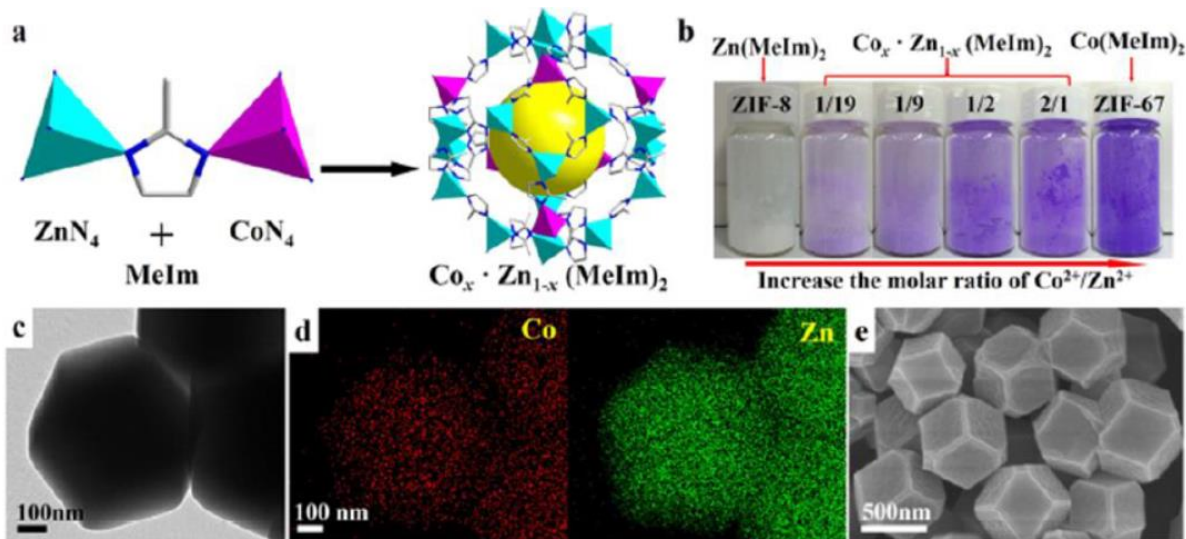
Figure 2.4 (a) Synthesis of Zn & Co based ZIFs, (b) coloring of various ratios of Zn & Co based ZIFs, (c) TEM images, (d) element mapping (e) SEM images of Zn & Co based ZIFs.[21].

In carbon and hybrid materials, metals play a significant role. Various MOF materials can serve as target materials with different metal ion compositions. The combination of metal ions with organic ligands in MOFs has the potential to effectively control the formation of metal oxide nanoparticles and deterioration of nanostructures in metal oxide nanoparticles. MOFs have a porous structure, which allows for many target materials or loading points for active compounds. The synthesis techniques are simple, and the conditions are mild, resulting in many different morphologies of the resulting materials, such as hollow polyhedra and spheres. For instance, PC and Co nanoparticles can be produced through the pyrolysis of 2-methylimidazoles of ZIF-67 into N-doped PC and Co nanoparticles. An and colleagues utilized a simple ZIFs-induced approach to synthesize Co/Co_3O_4 nanoparticle-coated PC core-shell. Furthermore, wet chemistry and high-temperature treatment created porous carbon polyhedrons from ZIF-8.
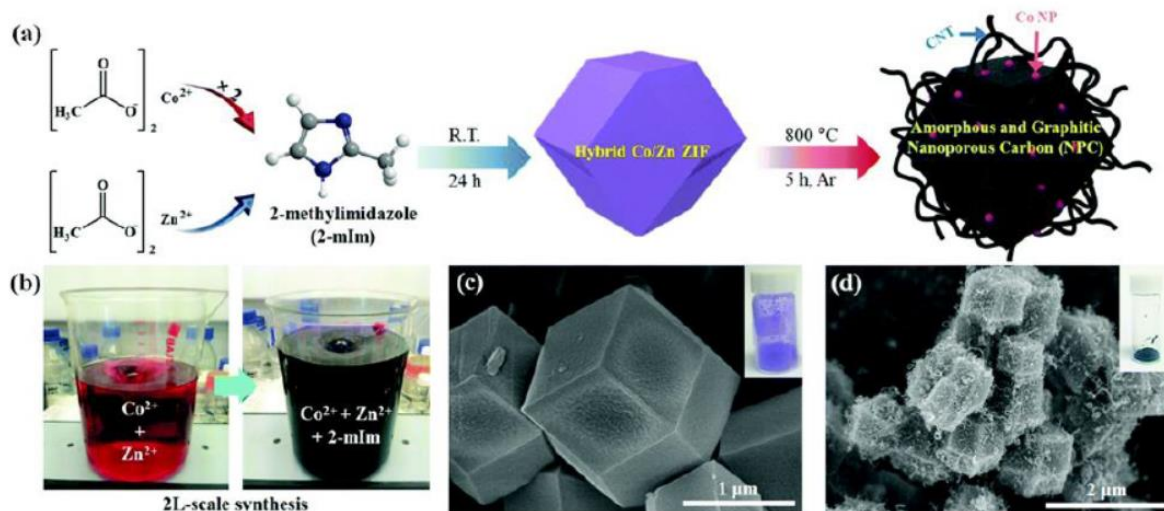
Figure 2.5 (a) synthesis scheme of Co/Zn based hybrid-ZIF to produce graphitic, (b) color of lab-scale production, (c & d) SEM images at different scales. [22].

2.2.3 Porous carbon and metal oxide-based ZIF composites

The composites of nanoporous carbon and metal oxides derived from ZIF are highly attractive due to their large surface area, which makes them an excellent architecture and precursor for energy storage applications involving high concentrations of carbon and nitrogen species. Structural changes in carbon derived from ZIFs can occur through activation and carbonization, which enable ion diffusion through the pores of their nanostructures. Effective electrochemical performance of the electrodes relies on the free ion diffusion. To this end, Yamauchi et al. developed an asymmetric supercapacitor using nanoporous carbon and nanoporous cobalt oxides (Co_3O_4) derived from ZIF-67. Carbon nanoparticles were generated from this precursor through the heat from nitrogen gas, which still decomposes organic matter when heated with air, resulting in nanoporous Co_3O_4. Remarkably, the parent MOF, ZIF-67, retained its original polyhedral shape in both situations, as depicted in Figure 2.6. Nanopores were found on the surface of nanoporous carbon, while the preparation of nanoporous Co_3O_4 involved random nanocrystals of 15-20 nm in size. As prepared, nanoporous carbons and nanoporous Co_3O_4 displayed surface areas of 350 and 1000 m^2/g, respectively. The Co_3O_4/carbon asymmetric supercapacitor has a very high specific energy and power of 36 Wh/kg and 8000 Wh/kg compared to the symmetric supercapacitors (carbon/carbon at 7 Wh/kg and Co_3O_4/Co_3O_4 at 8 Wh/kg).

21
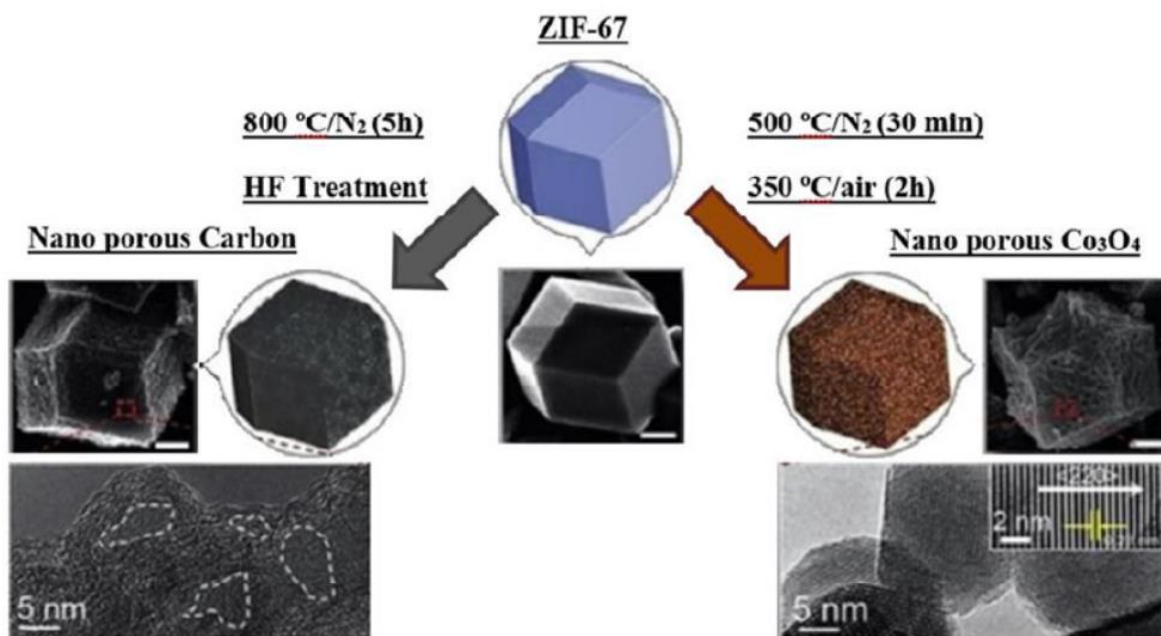
Figure 2.6 Carbonization and activation process to produce nanoporous carbon-based electrode material. [25].

2.2.4 ZIF-derived metal oxides/sulfides-based electrodes

Including a highly porous structure in the electrode can improve supercapacitor performance by facilitating the movement of electrolyte ions and increasing the electrode's capacitance. One potential method for achieving this is by growing or combining ZIF-derived porous carbon and metal complexes with conductive surfaces such as MoS_2. Another approach is to modify the active material-conductive substrate/additive linkage compound to improve electrode conductivity and active site count. Sulfur is a promising element for electrode materials due to its lower electronegativity value compared to oxygen, resulting in more stable compounds and faster electron movement.

Chen et al. demonstrated that self-supported Ni_3S_2 nanosheet arrays with high capacitance (1,000 F/g at 50 A/g) could be produced through the thermal breakdown of MOF precursors and subsequent sulfidation. NiS has also shown potential as an electrode material due to its high theoretical specific capacitance. Lou et al. employed an anion exchange technique and calcination of MOF precursors to produce hollow nanoparticles of NiS. Adding S^{2-} ions to ZIF-derived $NiCo_2O_4$ increased conductivity and super capacitance by increasing pore size and surface area.

22

The addition of S^{2-} ions also altered the structure of porous materials, making it easier for liquid electrolytes to enter. CoS nano boxes and Co_9S_8 hollow nanoparticles derived from ZIF-67 were also successfully synthesized and used in high-performance electrodes for supercapacitors[26].

2.2.5 ZIF-derived cobalt oxides and hydroxide electrodes

Among the many metal compounds available, cobalt oxide (Co_3O_4) is considered one of the best materials for supercapacitor electrodes due to its solid electrochemical activity, relatively low cost, and environmentally friendly properties, with a theoretical capacitance of 3600 F/g [25]. Cobalt hydroxide, another Co-based substance, has also garnered interest among researchers for its potential use in supercapacitor electrodes. By thermalizing MOF precursors with a layered structure and large inter-layer space, $Co(OH)_2$ can be formed, which exhibits fast ion movement, high redox reaction, and excellent stability, making it an ideal material for supercapacitor electrodes [12] Supercapacitors utilizing Co_3O_4 electrodes formed from nanoporous MOFs have been developed. Additionally, by carefully adjusting the synthesis procedures, it is possible to maintain the polyhedral shape of the MOF precursor, such as ZIF-67, within the Co_3O_4 framework. As a result of the nanoporous structure, the supercapacitors had improved current sweeps and were consequently more efficient. To create the porous hollow Co_3O_4 supercapacitor electrode, a double-walled tetrahedron MOF was selected because of its open architecture and high electrical conductivity. Figure 2.7 shows a ceria-based MOF and GO composite that outperforms the CNT-based composite.
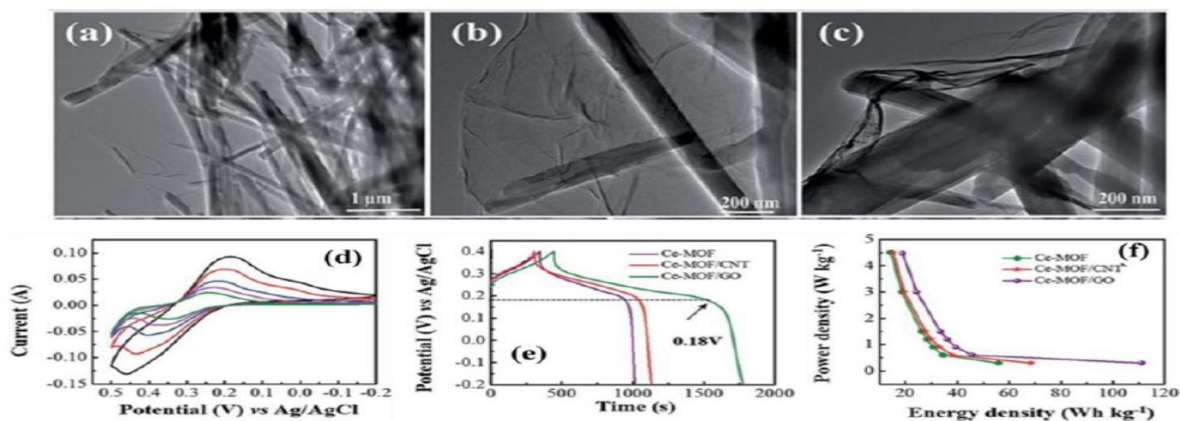
Figure 2.7 (a-c) TEM analysis of Ceria-based MOF/GO, (d-f) electrochemical analysis of Ceria-based MOF with GO in 3M KOH electrolyte along with Ragone plot of composite.

2.2.6 NiO-based composites

Activated carbon-Ni (OH)$_2$ hybrid cells can use NiO-carbon composites as a positive electrodes. When nickel oxide in an alkaline solution undergoes a redox reaction, the equation [21].

$$NiO \ + \ OH^- \ \leftrightarrow \ NiOOH + \ e^-$$
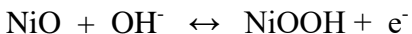
This is because the usual CV profiles of these materials cannot be used to calculate capacitance, which is why most literature is reported in F/g units. A wide electrochemical window must convert all reported capacities from F/g to mAh/g units. Three-dimensional (3D-RGNiO) nanoparticle composites were studied for their electrochemical behavior as battery electrode materials. It was made in 3 steps, which included the of NiO nanoparticles adsorption on the graphene and thermal treatment to decorate it. The 3D-RGNi composite has a higher specific capacity than the RG NiO and the 3D-RG composite. Aside from its good cycling stability, this composite electrode material has an 87 percent capacity retention after 2000 cycles. Large surface area and fast reaction kinetics were attributed to the porous structure of the graphene network [21].

Batteries with active materials based on carbon nanotubes or carbon nanofoam can also be implemented in supercapacitors. Using a one-step solvothermal process, a NiO nanoparticles composite on the surface of RG and CNTs was reported. More than twice as much specific capacity as pure NiO is delivered by this ternary composite in an electrolyte containing 6 M KOH, and it retains 94% of its capacity after 1000 cycles [27]

Summary

This chapter consists of a literature review on the types of electrode materials used for supercapacitor application. In addition, the performance of the electrode materials is also discussed in the chapter. Moreover, this chapter also contains the benefits and shortcomings of various MOF-derived materials for energy storage applications.

References

[1]   M. Jayalakshmi and K. Balasubramanian, "Simple capacitors to supercapacitors-an overview," *Int. J. Electrochem. Sci,* vol. 3, no. 11, pp. 1196-1217, 2008.

[2]   Y. Shao *et al.*, "Design and mechanisms of asymmetric supercapacitors," *Chemical reviews,* vol. 118, no. 18, pp. 9233-9280, 2018.

[3]   A. G. Pandolfo and A. F. Hollenkamp, "Carbon properties and their role in supercapacitors," *Journal of power sources,* vol. 157, no. 1, pp. 11-27, 2006.

[4]   S. Satpathy, S. Das, and B. K. Bhattacharyya, "How and where to use super-capacitors effectively, an integration of review of past and new characterization works on super-capacitors," *Journal of Energy Storage,* vol. 27, p. 101044, 2020.

[5]   M. Lu, *Supercapacitors: materials, systems, and applications*. John Wiley & Sons, 2013.

[6]   M. S. Halper and J. C. Ellenbogen, "Supercapacitors: A brief overview," *The MITRE Corporation, McLean, Virginia, USA,* vol. 1, 2006.

[7]   Y. Wang, Y. Song, and Y. Xia, "Electrochemical capacitors: mechanism, materials, systems, characterization and applications," *Chemical Society Reviews,* vol. 45, no. 21, pp. 5925-5950, 2016.

[8]   S. Cheng *et al.*, "Phase evolution of an alpha MnO2-based electrode for pseudo-capacitors probed by in operando Raman spectroscopy," *Nano Energy,* vol. 9, pp. 161-167, 2014.

[9]   P. Simon and Y. Gogotsi, "Materials for electrochemical capacitors," *Nature materials,* vol. 7, no. 11, pp. 845-854, 2008.

[10]   M. Salanne *et al.*, "Efficient storage mechanisms for building better supercapacitors," *Nature Energy,* vol. 1, no. 6, pp. 1-10, 2016.

[11]   Y. Wang and Y. Xia, "Recent progress in supercapacitors: from materials design to system construction," *Advanced materials,* vol. 25, no. 37, pp. 5336-5342, 2013.

[12]   Z. Wu, L. Li, J. m. Yan, and X. b. Zhang, "Materials design and system construction for conventional and new-concept supercapacitors," *Advanced science,* vol. 4, no. 6, p. 1600382, 2017.

[13]   Z. Li, J. Lin, B. Li, C. Yu, H. Wang, and Q. Li, "Construction of heteroatom-doped and three-dimensional graphene materials for the applications in supercapacitors: A review," *Journal of energy storage,* vol. 44, p. 103437, 2021.

[14] X. Yu, B. Lu, and Z. Xu, "Super long-life supercapacitors based on the construction of nanohoneycomb-like strongly coupled CoMoO4–3D graphene hybrid electrodes," *Advanced materials,* vol. 26, no. 7, pp. 1044-1051, 2014.

[15] J. F. Snyder, D. J. O'Brien, D. M. Baechle, D. E. Mattson, and E. D. Wetzel, *Structural composite capacitors, supercapacitors, and batteries for US Army Applications*. 2008.

[16] J. Chae, K. Ng, and G. Chen, "Nanostructured materials for the construction of asymmetrical supercapacitors," *Proceedings of the Institution of Mechanical Engineers, Part A: Journal of Power and Energy,* vol. 224, no. 4, pp. 479-503, 2010.

[17] W. Lu, J. Shen, P. Zhang, Y. Zhong, Y. Hu, and X. W. Lou, "Construction of CoO/Co-Cu-S hierarchical tubular heterostructures for hybrid supercapacitors," *Angewandte Chemie,* vol. 131, no. 43, pp. 15587-15593, 2019.

[18] H. Li *et al.*, "Quantifying the volumetric performance metrics of supercapacitors," *Advanced Energy Materials,* vol. 9, no. 21, p. 1900079, 2019.

[19] C. Liu, Q. Li, and K. Wang, "State-of-charge estimation and remaining useful life prediction of supercapacitors," *Renewable and Sustainable Energy Reviews,* vol. 150, p. 111408, 2021.

[20] M. Z. Iqbal, M. M. Faisal, and S. R. Ali, "Integration of supercapacitors and batteries towards high-performance hybrid energy storage devices," *International Journal of Energy Research,* vol. 45, no. 2, pp. 1449-1479, 2021.

[21] A. Allagui, A. S. Elwakil, B. J. Maundy, and T. J. Freeborn, "Spectral capacitance of series and parallel combinations of supercapacitors," *ChemElectroChem,* vol. 3, no. 9, pp. 1429-1436, 2016.

[22] L. Sun *et al.*, "Nitrogen-doped porous graphitic carbon as an excellent electrode material for advanced supercapacitors," *Chemistry–a european journal,* vol. 20, no. 2, pp. 564-574, 2014.

[23] H. Gualous, H. Louahlia-Gualous, R. Gallay, and A. Miraoui, "Supercapacitor thermal modeling and characterization in transient state for industrial applications," *IEEE Transactions on industry applications,* vol. 45, no. 3, pp. 1035-1044, 2009.

[24] Y. Zhan, Y. Guo, J. Zhu, and L. Li, "Power and energy management of grid/PEMFC/battery/supercapacitor hybrid power sources for UPS applications," *International Journal of Electrical Power & Energy Systems,* vol. 67, pp. 598-612, 2015.

[25] P. Forouzandeh, V. Kumaravel, and S. C. Pillai, "Electrode materials for supercapacitors: a review of recent advances," *Catalysts,* vol. 10, no. 9, p. 969, 2020.

[26] Z. S. Iro, C. Subramani, and S. Dash, "A brief review on electrode materials for supercapacitor," *Int. J. Electrochem. Sci,* vol. 11, no. 12, pp. 10628-10643, 2016.

[27] L. Zhang *et al.*, "Electrochemical ammonia synthesis via nitrogen reduction reaction on a MoS2 catalyst: theoretical and experimental studies," *Advanced Materials,* vol. 30, no. 28, p. 1800191, 2018.

Chapter 3: Review on Experimentation and Characterization Method

3.1 Synthesis Method

Various techniques have been developed to synthesize electrode materials in the laboratory, with some requiring specialized equipment and others being equipment-free. The selection of a particular electrode synthesis method depends on factors such as desired nanoparticle size, surface properties, and the type of material involved (e.g., semiconductors, metals, polymers, ceramics). Extensive research has been conducted to enhance the yield of the electrode, improve its structural properties, and increase its purity. Below are some of the methods that have been explored and refined.

3.1.1 Solvothermal Synthesis

Solvothermal synthesis is a versatile technique that can be utilized for producing a wide range of materials, including semiconductors, metals, polymers, and ceramics. This method involves the use of a solvent at moderate to high pressure (typically ranging from 1 atm to 10,000 atm) and temperature (ranging from 100 °C to 1000°C), which aids in the interaction of precursors during the synthesis process. When water is used as the solvent, the process is referred to as the "hydrothermal process." Hydrothermal synthesis is typically carried out at the supercritical temperature of water (374 °C). This method can be used to create various geometries, such as thin films, single crystals, bulk powders, and nanocrystals. Moreover, crystal formation (including rod (2D), sphere (3D), and wire (1D) shapes) can be controlled by adjusting factors such as the concentration of the chemical of interest, solvent supersaturation, and kinetics. Solvothermal synthesis can also be utilized to generate novel and thermodynamically stable forms of elements that are difficult to produce through other synthetic methods. Recent developments in solvothermal processes and nanocrystalline materials will be highlighted in this review, as over 80% of the literature in the last decade has focused on nanocrystals.

3.1.1 Synthesis of ZIF-67

The solvothermal method is commonly employed to prepare ZIF-67, while a simple approach is utilized for synthesizing ZIF-8. In this approach, cobalt nitrate hexahydrate (a metal salt) is mixed with methanol to form a solution, while a separate solution of 2-methylimidazole (an organic linker) is prepared by mixing it with methanol. The ratio of the metal salt and organic linker is adjusted depending on the desired morphology and intended application. These two solutions are then combined at room temperature and stirred for 30 minutes. After stirring, the solution is aged for 24 hours, resulting in the formation of a purple precipitate that settles at the bottom. The precipitate is thoroughly washed with ethanol and deionized water before being collected and dried in a vacuum oven at 60°C for 12 hours. Once vacuum drying is complete, the sample is ground to obtain a fine powder.

3.1.2 Hydrothermal Synthesis

The synthesis method discussed here is ideal for creating materials that demand specific synthesis conditions. This technique facilitates control over the material's morphology, structure, and other properties. It is particularly useful for synthesizing metal oxides, halides, and composites that require precise temperature and pressure conditions. The nanoparticles generated through this approach possess unique properties. Typically, an autoclave device is utilized during this method, allowing for simultaneous control of temperature and pressure. The most significant advantage of this process is its cost-effective ability to synthesize a broad range of NPs with upgraded composition, size, structure, and surface chemistry.

3.1.3 Pyrolysis

During pyrolysis, organic matter is decomposed into no condensable gases, condensable liquids, and biochar or charcoal as a residual solid product in an inert environment without oxygen.

3.1.4 Carbonization

Carbonization is a thermal decomposition process that produces a carbonaceous residue by removing the distillate from organic substances. Pyrolysis, the oldest method of directly producing liquids from coal, involves heating coal and capturing the volatilized liquids, resulting in a hydrogen-depleted carbon residue. However, due to the production of a small amount of liquid (less than 20%), and a mixture of chemicals and water contamination, the resulting product is of low quality. While organic matter undergoes decomposition at high temperatures and distillate is

removed simultaneously, carbonization is primarily used to produce a carbonaceous residue, commonly referred to as coke. In the case of ZIF, carbonization is performed to transform it into nano-porous carbon and carbon nanotubes.

3.2 Characterization Techniques

3.2.1 X-Ray Diffraction (XRD)

X-ray diffraction (XRD) is a commonly used and significant technique for material characterization that provides information on the material's morphology, components, and crystallite size. It involves passing X-ray radiations at an angle through the material from a source, calculating the diffraction angle, and recording the intensity. By measuring how many radiations deflect from a specific plane on the material, XRD provides information on the structure and morphology of the material.

XRD is based on the double particle/wave nature of X-rays, and its primary purpose is the identification and characterization of materials based on their X-ray form. When monochromatic X-rays hit an object material, the atoms in the target scatter the X-rays, causing diffraction in crystalline materials. The diffraction pattern is described by Bragg's Law,

$$n(\lambda) = 2d\ Sin(\theta) \qquad (1)$$

where the number of wavelengths equals twice the distance between crystal planes times the sine of the diffraction angle.

The size and shape of the unit cell determine the directions of likely diffractions, and the arrangement of atoms in the crystal structure affects the intensities of the diffracted waves. Most materials are not single crystals, but rather are composed of small crystallites in all possible directions, known as polycrystalline powder or aggregate. When a material with randomly oriented crystallites is exposed to X-rays, the beam will view all available interatomic planes, and adjusting the experimental angle will allow for the identification of all available diffraction peaks from the substance.
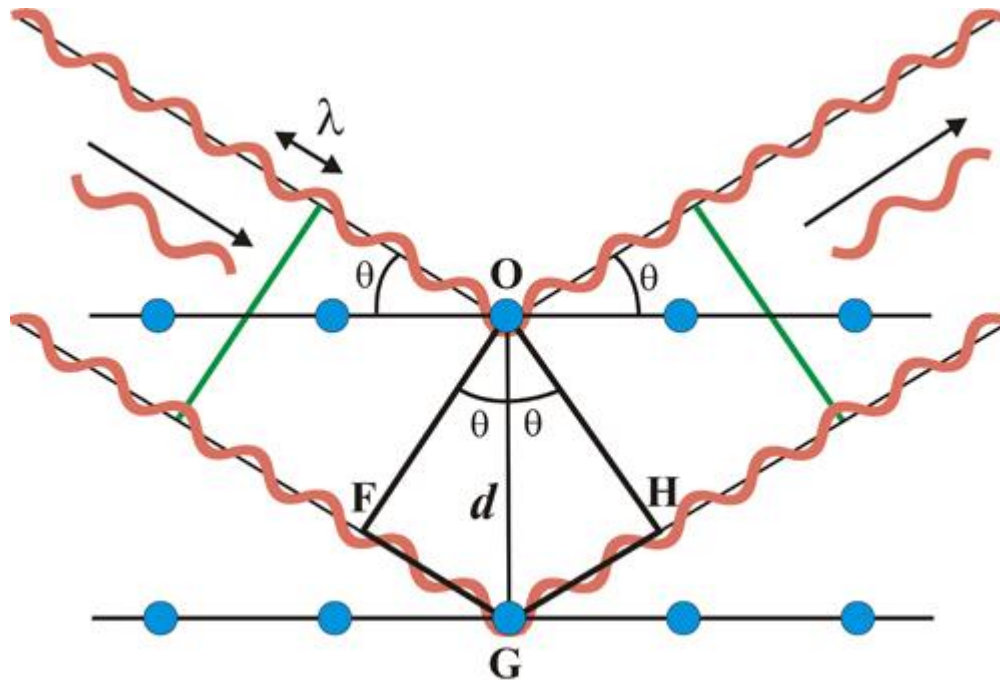
Figure 3.1 Bragg's Law

3.2.2 Scanning Electron Microscopy (SEM)

The SEM is an instrument that utilizes a focused beam of high-energy electrons to generate multiple signals from the surface of a solid specimen. These electrons penetrate through the material and exit from the other end, as illustrated in Figure 3.2. By analyzing the interactions between the electron beam and the sample, the SEM can provide information on the substance's chemical composition, crystalline structure, external morphology, and material orientation. The SEM can create a 2-dimensional image that displays spatial variations in properties, and data can be collected over a specific area of the sample surface.

This scanning method, which typically offers a magnification range of 20X to approximately 30,000X and a 3D resolution of 50 to 100 nm, is useful in distinguishing areas that vary in size from approximately 1 cm to 5 microns in width.

The SEM is particularly valuable in identifying chemical contents (by EDS), crystal orientations (using EBSD), and crystalline structure. It can analyze a specific area or point location on the sample object, much like the EPMA, and shares many similarities in design and function.
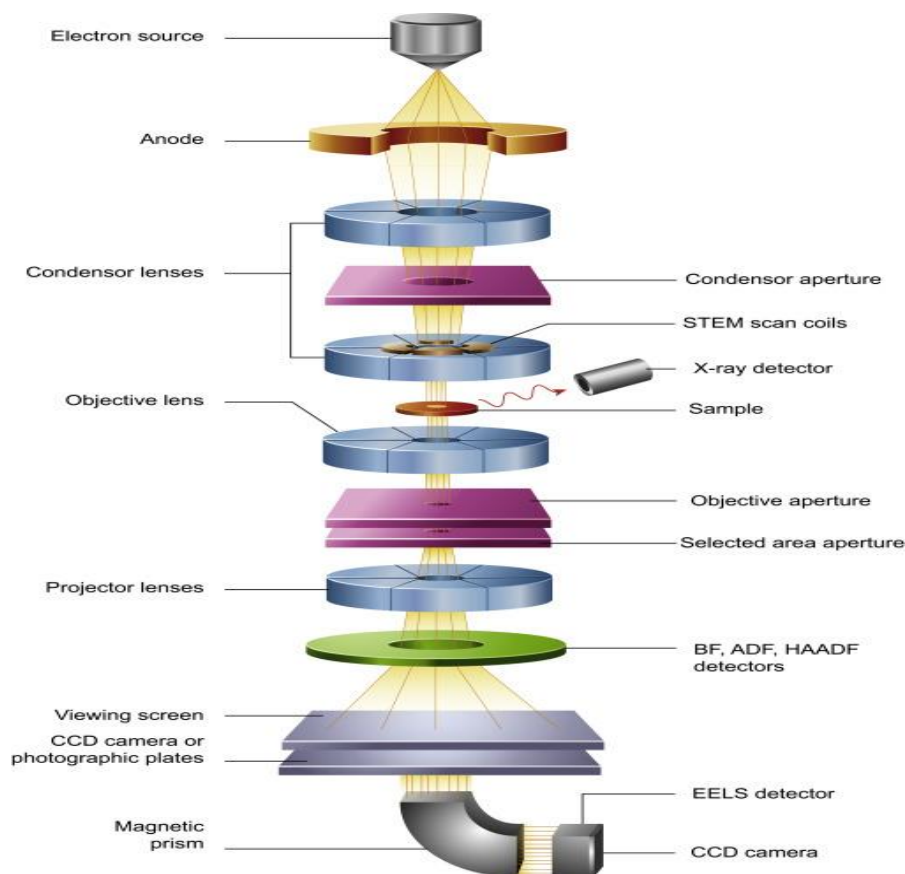
Figure 3.2 Scanning Electron Microscopy

3.2.3 Energy Dispersive X-ray Spectroscopy (EDX)

EDS is a method of analyzing elements that can determine the number of individual elements present in a nanoparticle. This technique provides information on the substances present at a specific point but does not indicate the overall quantity of each element. EDS is often combined with SEM or TEM to obtain a nanoscale image of particles, with EDS performing the analysis of the nanostructure. In the early 1970s, EDS became a commercial product and quickly surpassed WDS in popularity. EDS has a simple overall structure, with no moving parts like the rotation detector in WDS. The sensor collects X-ray energy signals from all series elements in a sample at the same time, unlike the collection of signals from X-ray wavelengths one by one, making EDS systems relatively fast, as shown in Figure 3.3. The characteristic energy dispersion resolution of EDS is around 150-200 eV, which is lower than WDS resolution. The lightest component that can be identified is not C (Z=6), but O (Z=8). However, the major advantages of EDS, such as low cost and fast analysis, render these disadvantages insignificant. The EDS band is a graph that

33

depicts the relationship between the power of X-rays and the corresponding energies. Both light and heavy elements can be observed within a range of spectrum from 0.1 to 10-20 keV since both the M or L lines of heavy elements and the K lines of light elements are present in this range.
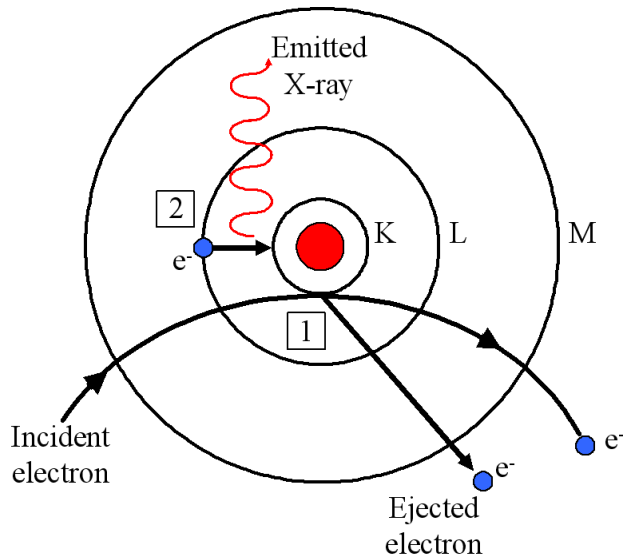
Figure 3.3 Illustration of EDX

3.2.4 Thermo-Gravimetric Analysis

Thermo-gravimetric analysis (TGA) determines weight losses in a material with a change in temperature in a controlled atmosphere. The major applications of this characterization technique are the measurement of thermal stability, volatile content, moisture, organic linker in a sample, and the percent composition of components in a compound. The principle is that the temperature is gradually increased from zero to the required final temperature in a specific gas atmosphere which maybe Ar, air or some other gas. Now when temperature increases the contents in the sample start to evaporate. Moisture is usually the first content that removes from the sample so a change in mass of sample occurs. This mass is measured on the weight balance continuously during the process which is placed outside the furnace Figure 3.4. After moisture other volatile contents like organic residues start to escape. The stability of the sample can be defined as the temperature at which the material starts to decompose which is the main point in the curve. After that the line drops sharply causing a major loss in material. This point is called the decomposition temperature and determines the stability of material. The weight of the material is mapped against temperature

or time to demonstrate the thermal changes in the sample, for instance, the loss of solvent, loss of water of hydration, and the decomposition of the material. At the end of the process, the final mass residue is noted, and the total mass loss is calculated.
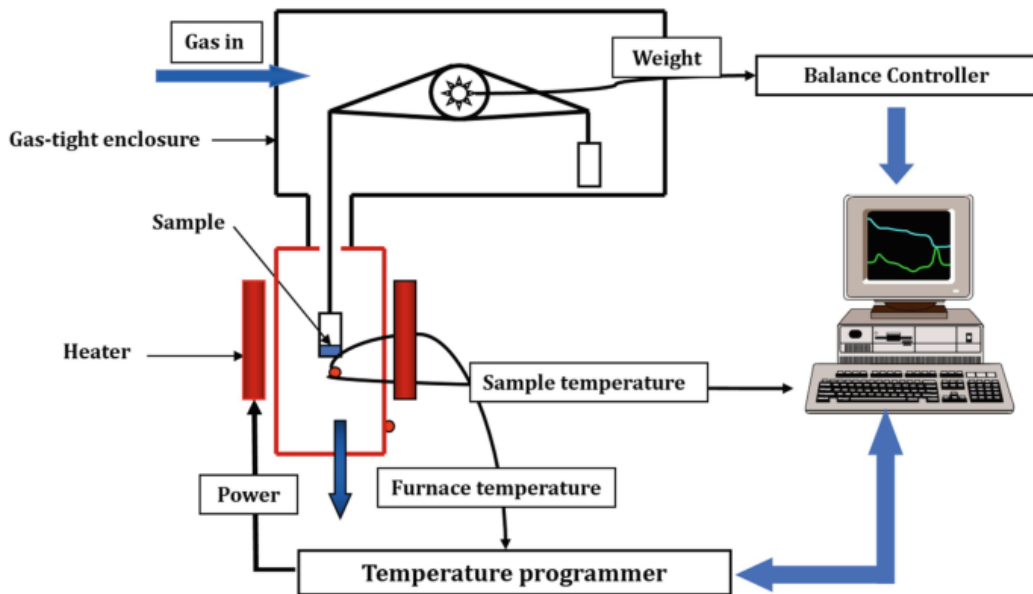
Figure 3.4 Illustration of TGA

3.3 Electrochemical Testing

3.3.1 Slurry/Ink Formation

There are many substrates available for using as working electrode for example Glassy carbon electrode, nickel foam and carbon cloth. For every substrate method of ink formation is different. For glassy carbon we use ethanol as solvent and nafion (5 wt.% ion solution in lower aliphatic alcohols) as binder. Purpose of binder is to bind the active electrode material so that it sticks to the electrode. For nickel foam and carbon cloth we use PVDF as binder and n-methylepropyrilidine (NMP) as solvent. Carbon black/graphite powder/super-p is also added to the slurry. PVDF binder causes resistance that ultimately mitigate the overall conductivity of the active material. Purpose of carbon black is to cope with the reduced activity of active material caused by the PVDF binder. After mixing the required recipe, solution is sonicated for 4 hours to make homogenous suspension.

3.4 Electrochemical Techniques

When glassy carbon electrode is fabricated, it is dried at 60 degrees Celsius for 30 minutes. After that electrochemical testing is performed. For Supercapacitors three techniques are performed in electrochemical workstation.

- Cyclic Voltammetry (CV)

- Chronopotentiometry

- Electrochemical Impedance Spectroscopy (EIS)

3.4.1 Cyclic Voltammetry

Cyclic voltammetry (CV) is a great and common technique of electrochemistry usually used to study the oxidation and reduction procedures of molecular species. It is helpful to investigate chemical reactions initiated by electron transfer, which comprises catalysis. This electrochemical technique involves the running of the workstation through a complete cycle. The potential range was input into the software which is applied across the two electrodes. Scan rate, sample interval, sensitivity was given for each run along with several segments. Two segments make one complete cycle. The cyclic voltammetry gives information of the current changing with voltage as shown in Figure 3.6 [10]. When CV is performed the current passes through an external circuit and electrons start to flow from anode to cathode. For CV, beaker cell was used in three electrode system. Working electrode was glassy carbon, counter electrode was platinum wire and reference electrode was Ag/AgCl [6].
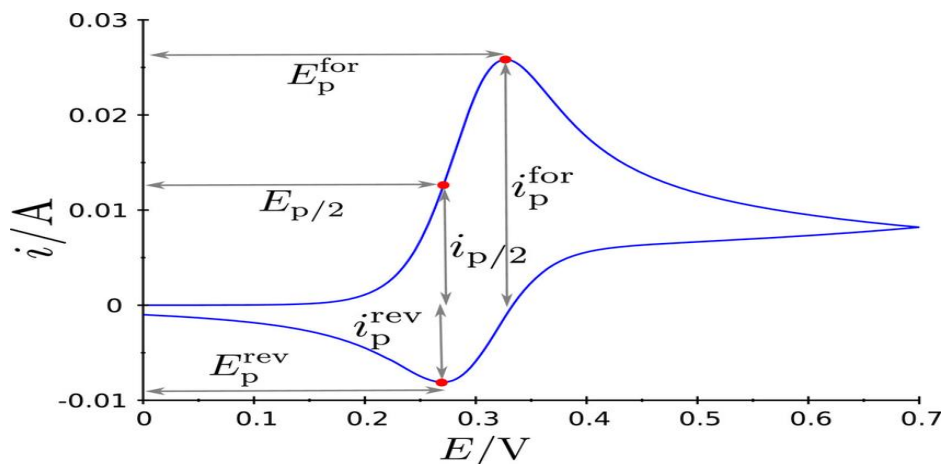
Figure 3.5 CV profile.

3.4.2 Chronopotentiometry

Chronopotentiometry is an electrochemical analysis method where the electrodes are subjected to a constant flow of current in order to the cause a constant reduction of the electroactive material Figure 3.7. This method is differentiated from constant-current coulometric analysis and coulometric titrimetry1 because in this technique the applied current appears to be significantly large so that the efficiency of current required for the reduction of the material is reduced below 100% within a few seconds.
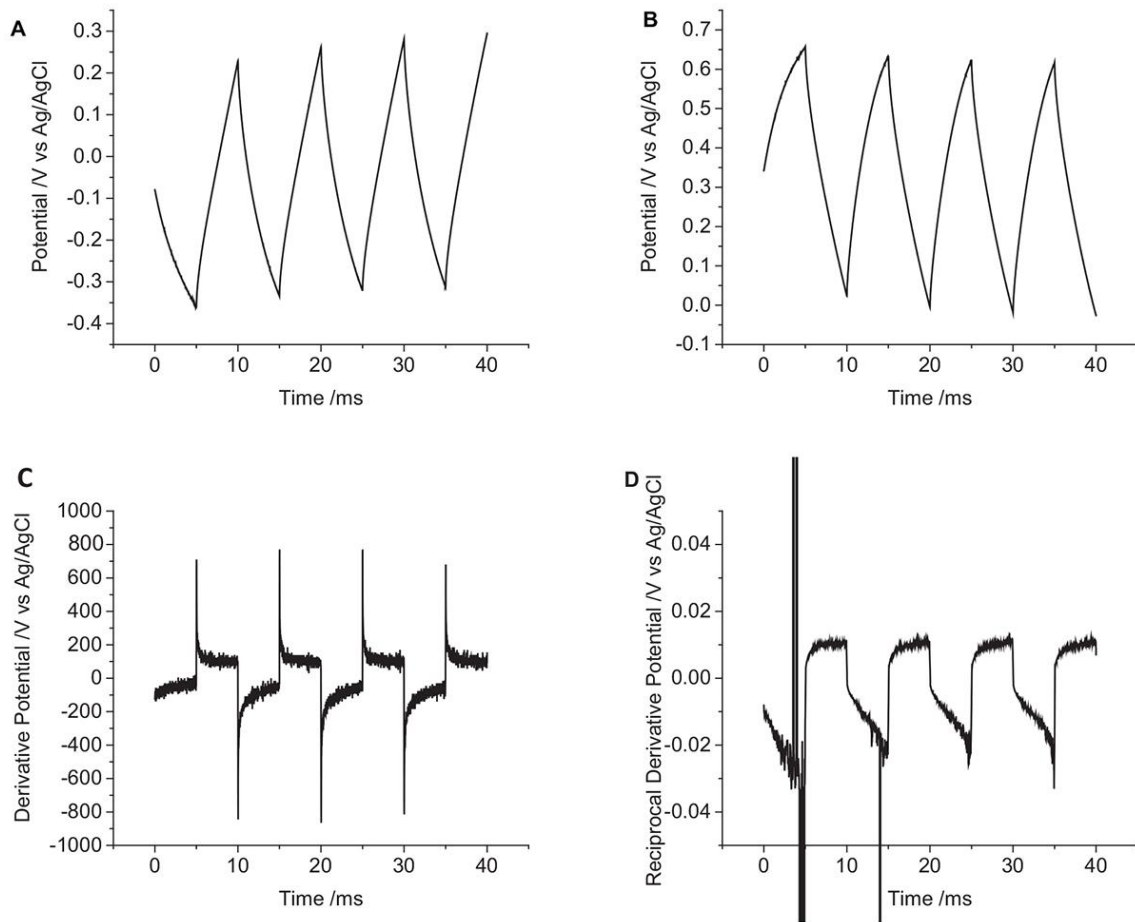
Figure 3.6 Chronopotentiometry Profile.

3.4.3 Electrochemical Impedance Spectroscopy (EIS)

This technique of electrochemical workstation allows us to measure the resistivity of our system. This includes resistance of electrolyte, ohmic loss and or activation losses. Electrical resistance is the measure of the of a circuit element that resists current flow.

$$R = E/I \tag{2}$$

According to Ohm's law, R is the resistance which is defined as the ratio of voltage (E), and current (I). This known law use is limited to only one circuit element, the ideal resistor.

An ideal resistor has several simplifying properties:

- Ohm's Law is followed at every range of current and voltage.

- Resistance is not dependent on the frequency.

- The voltage passing through a resistor and the AC current are in a single phase.
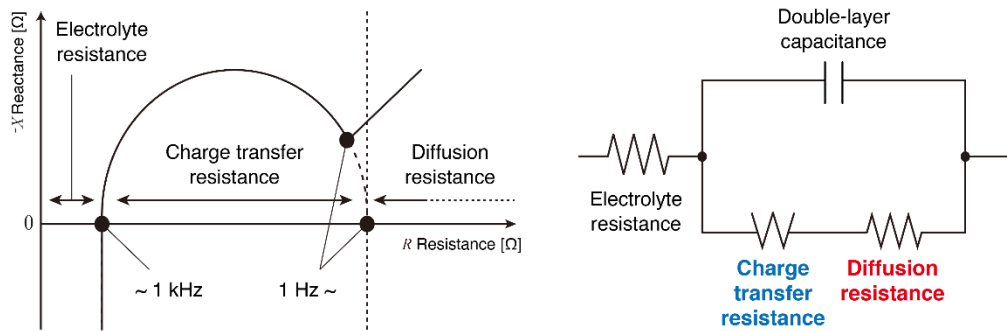
Figure 3.7 EIS Profile (Nyquist Plot).

3.5 Electrochemical Parameters

The determination of the energy density and power density is very important to evaluate the efficiency of a supercapacitor for real-life applications. Cyclic voltammetry (CV) and chronopotentiometry are the techniques that can confirm the energy and power densities by using the following equations:

The specific capacitance (C, Fg^{-1}) can be determined using cyclic voltammetry:

$$C_s = \frac{\int IdV}{2mv\Delta V} \tag{3}$$

Here, $\int IdV$ is the integral area of the CV curves, m represents the mass, n represents the scan rate used to perform the analysis, and the voltage window of the process is represented by V.

$$E = \frac{1}{2}\frac{C_m \Delta V^2}{3.6} \qquad (4)$$

Here, E is the symbol for energy density. The specific power (W/kg) defines how rapidly a device is able to deliver energy under a constant current density to external loads. The maximum specific power is calculated as:

$$P = \frac{E}{\Delta t} \times 3600 \qquad (5)$$

Here, P represents the maximum power that can be achieved by a supercapacitor.

3.6 Summary

This chapter initially discusses different chemical synthesis methods like solvothermal and hydrothermal method. After that material characterization techniques have been studied i.e., XRD, SEM, EDS, TGA, BET. Main principle of these techniques has been noted down along with diagrams. After that the whole electrochemical testing process implemented was explained including ink formation, ink deposition on substrate and electrochemical performance determination using various techniques like CV, CP, and EIS with a three-electrode system.

References

[1]   T. Takahashi, K. Kuwabara, and M. Shibata, "Solid-state ionics - conductivities of Na+ ion conductors based on NASICON," *Solid State Ionics*, vol. 1, no. 3–4, pp. 163–175, 1980, doi: 10.1016/0167-2738(80)90001-6.

[2]   N. S. Mohamed, R. H. Y. Subban, and R. Rusdi, "Enhancement of electrical properties of NASICON-type solid electrolytes (LiSn2P3O12) via aluminium substitution," *J. Sci. Adv. Mater. Devices*, vol. 5, no. 3, pp. 368–377, 2020, doi: 10.1016/j.jsamd.2020.06.003.

[3]   F. Zheng, M. Kotobuki, S. Song, M. O. Lai, and L. Lu, "Review on solid electrolytes for all-solid-state lithium-ion batteries," *J. Power Sources*, vol. 389, no. April, pp. 198–213, 2018, doi: 10.1016/j.jpowsour.2018.04.022.

[4]   C.J.Brinker;G.W.Scherer,"Sol-Gel_Science_The_physics_and_chemistry_of_sol-gel_processing_-_Brinker_1990.pdf." p. 462, 1990. doi: 10.1016/S0254-0584(02)00315-2.

[5]   S. D. Lee *et al.*, "Composite Electrolyte for All-Solid-State Lithium Batteries: Low-Temperature Fabrication and Conductivity Enhancement," *ChemSusChem*, vol. 10, no. 10, pp. 2175–2181, 2017, doi: 10.1002/cssc.201700104.

[6]   J. Lai, W. Niu, R. Luque, and G. Xu, "Solvothermal synthesis of metal nanocrystals and their applications," *Nano Today*, vol. 10, no. 2, pp. 240–267, 2015, doi: 10.1016/j.nantod.2015.03.001.

[7]   X. Dong, M. Qi, Y. Tong, and F. Ye, "Solvothermal synthesis of single-crystalline hexagonal cobalt nanofibers with high coercivity," *Mater. Lett.*, vol. 128, pp. 39–41, 2014, doi: 10.1016/j.matlet.2014.04.133.

[8]   S. Sōmiya and R. Roy, "Hydrothermal synthesis of fine oxide powders," *Bull. Mater. Sci.*, vol. 23, no. 6, pp. 453–460, 2000, doi: 10.1007/BF02903883.

[9]   S. Feng and R. Xu, "New materials in hydrothermal synthesis," *Acc. Chem. Res.*, vol. 34, no. 3, pp. 239–247, 2001, doi: 10.1021/ar0000105.

Chapter 4: Methodology and Experimentation

4.1 Experimental

4.1.1 Synthesis of Co/NPC:

Firstly, ZIF-67 was prepared by co-precipitation method. 1.97g of 2-MIM and 1.746 g of cobalt nitrate hexa-hydrate ($Co(NO_3)_2 \cdot 6H_2O$) was dissolved in 30ml of methanol separately and stirred for 1 hour on a hotplate. After the solutions were completely dissolved in methanol the two solutions were mixed and again stirred for an hour. After stirring the final solution was left for 24 hours at room temperature, for aging purpose. After that the precipitates of ZIF-67 was collected by filtration on a watt man filter paper and washed several times with ethanol and then dried at $60^{o}C$ in a heating oven. The dried and well ground material was then pyrolised at $800^{o}C$ for 3hrs in a tube furnace with a ramp rate of $5^{o}C$ in Ar/H_2 (90:10 mixture) environment. After pyrolysis the black particles were collected and grinded to be used further[1].

4.1.2 Synthesis of ZIF-67/NPC/MoS₂ Composites:

The as prepared ZIF-67/NPC was then utilized to form ZIF-67/NPC/MoS_2 composites. 2mmol of sodium molybdate and 10mmol of Thioacetamide was added in a 30ml of DI water and sonicated. ZIF-67/NPC was separately sonicated in 30ml DI water. After that both the solutions were mixed and the resulting solution was again sonicated. After that the final solution was poured into a 100ml Teflon lined autoclave and kept in a heating oven at $200^{o}C$ for 36hrs. After heating the autoclave was kept at room temperature for overnight. The black precipitates were then filtered and dried at $80^{0}C$ for 12hrs.[1]
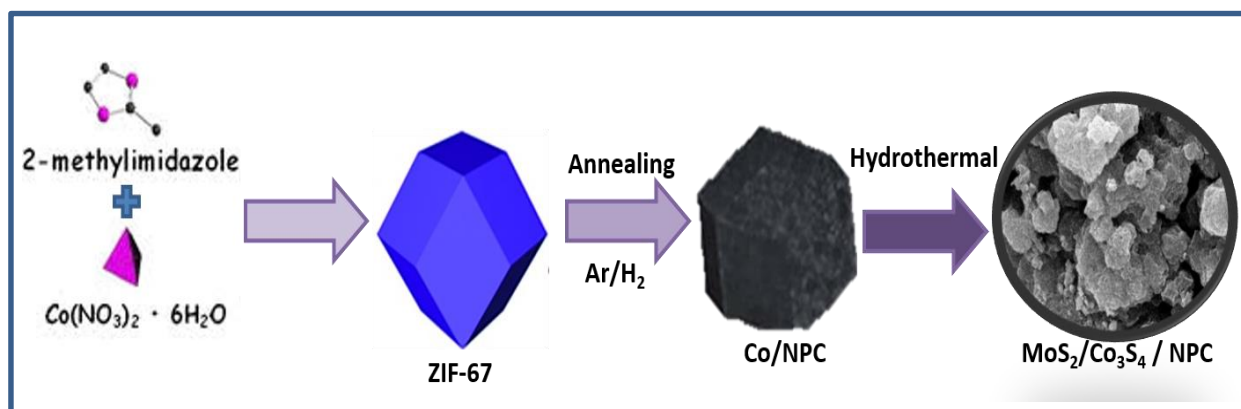
Figure 4.1 Schematic diagram of Synthesis technique

Using the same preparation technique three samples with different molar mass of Co/NPC was prepared. The molar mass of Co/NPC was varied to check the effect of different ratios of the two metals (Molybdenum and Cobalt). The final three composites were abbreviated as CMS in whole manuscript. Table 1 shows the molar masses were to make different ratios. The amount of Thioacetamide (sulfur source) was kept constant(10mmol) in all the three samples.

Table 1 Molar ratio of Mo and Co in CMS-1, CMS-2 and CMS-3

	Mo	**Co/NPC**	**Mo:Co**
CMS-1	2mmol	1mmol	1:0.5
CMS-2	2mmol	2mmol	1:1
CMS-3	2mmol	4mmol	1:2

4.2 Material Characterization:

The morphologies and micro-structure of the prepared materials were characterized with analytical scanning electron microscopy (JEOL JSM-6490A). Structural analysis was performed using X-ray powder diffraction (D8 Advance by Bruker Germany). Raman Spectroscopy was performed at an Apollo Raman (BWTEK (BWS415-532S) to confirm the carbon presence in the material. Surface area and pore size were analyzed using Brunner–Emmet–Teller (Quantachrome Novawin 2200 Instrument) technique. Thermo-gravimetric analysis (TGA) was accomplished in N_2 environment by using Discovery TGA 5500 (TA Instrument, USA).

4.3 Electrochemical Testing:

All the measurements were performed by using CHI (E760) electrochemical workstation. The working electrode was prepared on Nickel foam. Firstly, Nickle foam was washed with HCL, DI water and ethanol. Then using a 1mg PVDF binder solution with active material a homogeneous slurry was prepared and drop casted on a (1 cm x 2 cm) piece of Nickle foam. The actual mass loading was measured by subtracting the weight of Nickle foam before and after the fabrication process. The following mass loading values were obtained CMS-1, CMS-2, CMS-3 0.003g/cm^2, 0.00165g/cm^2 and 0.002527g/cm^2, respectively. The electrochemical testing was done on a three electrode system using, platinum and Ag/AgCl as counter and reference electrodes, respectively. 1M KOH was used as electrolyte solution. CV test were run between a voltage range of 0-0.45V on different scan rates. Similar voltage window was used for performing GCD on different current densities.

References

[1]   X. Zhang, F. Zhou, S. Zhang, Y. Liang, and R. Wang, "Engineering MoS2 basal planes for hydrogen evolution via synergistic ruthenium doping and nanocarbon hybridization," *Advanced Science,* vol. 6, no. 10, p. 1900090, 2019.

Chapter 5: Results and Discussion

5.1 Structural and Morphology Analysis

The morphology and structure analysis were performed using scanning electron microscopy (SEM). The SEM image of pure ZIF-67, prepared through co-precipitation method, shown in Fig.2 (a), hexagonal structure of ZIF-67 in the SEM image confirms the formation of ZIF-67 with an average particle size of (particle Size). Fig.2 (b) shows the SEM image of ZIF-67 after pyrolysis at 800 °C in Ar/H$_2$ mixture, porous surface and disrupted morphology of ZIF-67 can be seen. SEM images of CMS-1, CMS-2 and CMS-3 after hydrothermal treatment with Mo and S shown in Fig.5.1 (c, d, e) shows a complete disruption of structure with agglomeration. Sulfur causes a layer on the material particles causing structure deformation and agglomeration. EDX in Fig.5.1 (f) shows the atomic and mass percent ratios of different element present in CMS-2. EDX confirms the presence of C, Mo, S and Co in the prepared sample. EDX of CMS-1 and CMS-3 is shown in supplementary data.

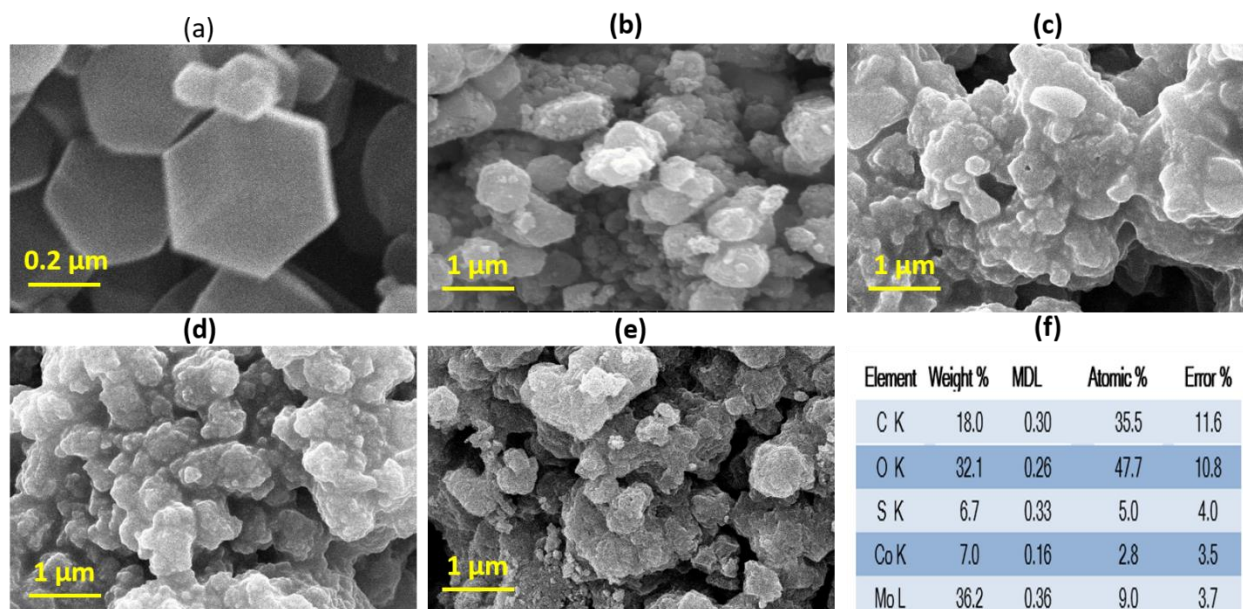| Element	Weight %	MDL	Atomic %	Error %
C K	18.0	0.30	35.5	11.6
O K	32.1	0.26	47.7	10.8
S K	6.7	0.33	5.0	4.0
Co K	7.0	0.16	2.8	3.5
Mo L	36.2	0.36	9.0	3.7

Figure 5.1 SEM images of (a) ZIF-67, (b) ZIF-67 pyrolized@800°C, (c) CMS-1, (d) CMS-2 (e)CMS-3, (f) EDX CMS-2

The synthesized materials were investigated by XRD and the characteristic peaks of the three materials are shown in **Fig.5.2 (a)** The characteristic peaks at 29°, 35.85°, 38.58°, 40.89° and 58.1° can be indexed to (004), (102), (103), (103) and (110) planes of hexagonal MoS_2, respectively. (JCPDS No. 37-1492).[27-29] in CMS-1. While the peaks at 18.38°, 26.9° and 55.1° can be attributed to the (111), (220) and (440) planes of Co_3S_4 (JCPDS card number 47–1738). [30, 31]. We can observe a peak at 2θ value of 44.02° which can be indexed to the (111) peak of metallic cobalt, hence proving the pyrolysis of ZIF-67. A sharp peak of MoO_2 (011) is present at 26.2°. The high intensity of this peak is due to the co-existence of broad peak of graphitic carbon and Co_3S_4 at the same values. So as a result we see a high intensity peak of MoO_2. In XRD pattern of CMS-3 we see a different phase of cobalt sulphides the peaks at 2θ 20.2° and 52.2° are the peaks of (111) and (420) plane of Co_9S_8 (JCPDS card number 19-0364). The metallic cobalt peak at 44.2 is also present however we do not see any clear peak of MoS_2 in this sample which is due to the amorphous nature of MoS_2 [32] in CMS-3. However, a clear broad peak of graphitic carbon can be seen at 26.2°. The XRD pattern of CMS-3 is also well matched with the pattern of MoS_2/Co_9S_8 CNTS [33] so the disappearance of MoS_2 peaks can be due to excess formation of CNTs in CMS-3.
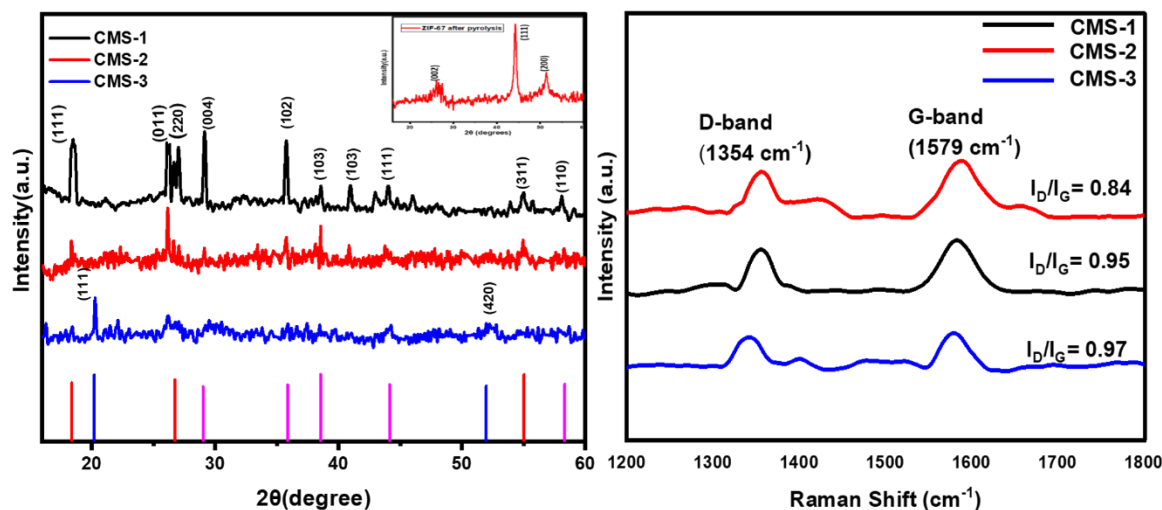

Figure 5.2 (a) XRD pattern of CMS-1, CMS-2 and CMS-3 (b) Raman spectra of CMS-2

Raman spectra of the sample CMS-2 is present in Fig. 3 (b) D and G band of the graphitic carbon are present around 1350 cm^{-1} and 1580 cm^{-1}. Normally, the D band is associated with disordered

atoms defects in sp^2 <u>hybridized carbon</u>, whereas the G band is related to sp^2-bonded carbon in graphitic structures. The I_d/I_g ratio of three samples CMS-1, CMS-2, CMS-3, were 0.88, 0.83, and 0.87 respectively. The I_d/I_g ratio of 0.83 shows the high degree of defects in graphitic carbon in CMS-2. The low I_D/I_G ratio value has a positive impact on the increase in electrical conductivity.[34] The comparitive graph of raman shift of three samples is shown in supplementary data.

The materials' adsorption characteristics and surface area were examined using the N_2 adsorption/desorption technique. Fig.5. (a) displays the BET isotherms of CMS-1 and CMS-2. The sample's isotherms are all type 4 isotherms having mesopores. As shown in Fig.5. (a), CMS-1 and CMS-2 have surface areas of 40 m^2 g^{-1} and 98 m^2 g^{-1}, respectively. The rise in ZIF-67-NPC's molar mass indicates an increase of 60%. It might lead to improved CMS-2 electrochemical performance. The pore radius was calculated using the desorption portion of the Barrett-Joyner-Halenda (BJH) pore size distribution, as illustrated in Fig. 5(b). Fig. shows that the pore radii range from 1.5 nanometers to 8.2 nanometers. Pore volume was discovered to be 0.066 cm^3 g^{-1} for CMS-1 and to be 0.13 cm^3 g^{-1} for CMS-2. A high total pore volume can encourage the electrolyte's diffusion within the material, which helps the redox reaction continue fast and effectively.[30]
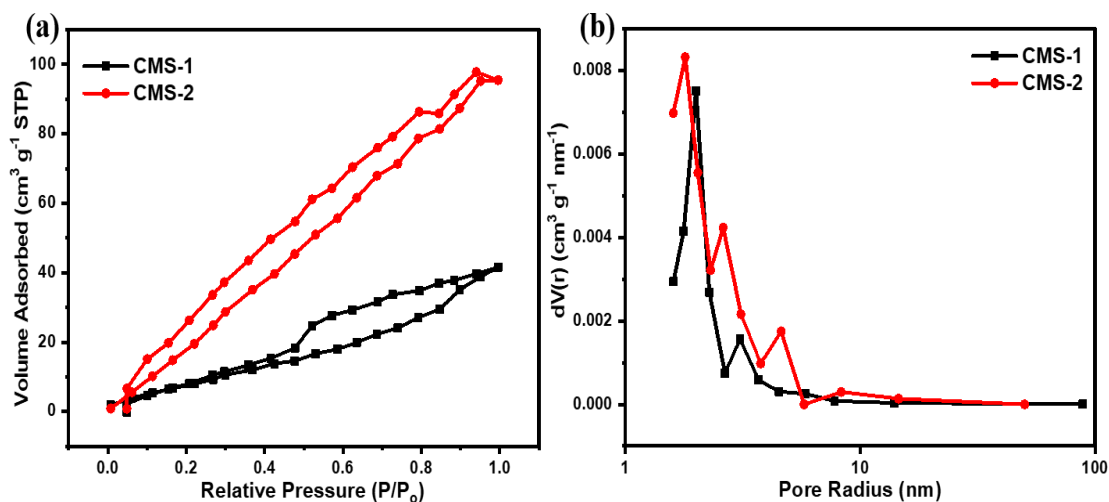

Figure 5.3 (a) BET Isotherm's of CMS-1, CMS-2 (b) Pore size distribution curve of CMS-1 & CMS-2

5.2 Electrochemical Measurement

The electrochemical testing was performed in an electrolyte solution of 1M KOH using cyclic voltametery(CV), galvanostatic charge discharge(GCD), and electrochemical impedence spectroscopy. CV was performed in a potential window of 0-0.45 at different scan rates, 1 m vs^{-1} to 20 m vs^{-1}. The CV curves of three samples obtained at different scan rates are shown in Fig.6.(a,b,c) a comparitive analysis of the three samples is also shown in Fig.6.(d). when the scan rate increase from 1 m Vs^{-1} to 20 m Vs^{-1} the area under the curve increases due to the increase in current density. All the curves show a pair of redox peaks and maintain its shape, indicating typical pseduocapacitive behaviour governed by faradic redox reaction and good rate capability. Co_3S_4 and MoS_2 are typical pseudo-capacitive materials, all of which provide capacitance in <u>alkaline electrolyte</u>.[36] A specific capacitance of 594 F g^{-1}, 612 F g^{-1} and 421 F g^{-1} is achieved by CMS-1, CMS-2 and CMS-3 The specific capacitance decreases with the increase in scan rate. At lower scan rates the positive ions of electrolyte can easily diffuse into all spaces of the electrode while at high scan rate the ions can only reach the surface material of the electrode having little contribution from the material embedded in the electrode.[37] CMS-2 having equal molar ratio of Mo and Co have shown highest specific capacitance. Indicating CMS-2 as the optimum ratio sample. The high specific capacitance can be attributed to the high surface area in BET isotherm of CMS-2. When the molar ratio is increased to double in CMS-3 we see that the specific capacitance decreases. This drop in capacitance can be attributed to the formation of Co_9S_8 phase in CMS-3 as Co_9S_8 phase of cobalt sulphides has much lower conductivity than Co_3S_4 phase.[38] Moreover the CV curve shape of CMS-3 shows a prominent effect of EDLC behavior ,due to high percentage of carbon, and hence have a lower specific capacitance as compared to other materials, which are more inclined to pseudo-capacitive behavior. Pseudo-capacitance is 10 to 100 times more than EDLCs.[39] Fig.6.(d) shows a comparative CV behavior of three samples. The smaller area under the curve of CMS-2 is due to the difference in mass loading of the three electrode as explained by Ahmad et al. in [34]
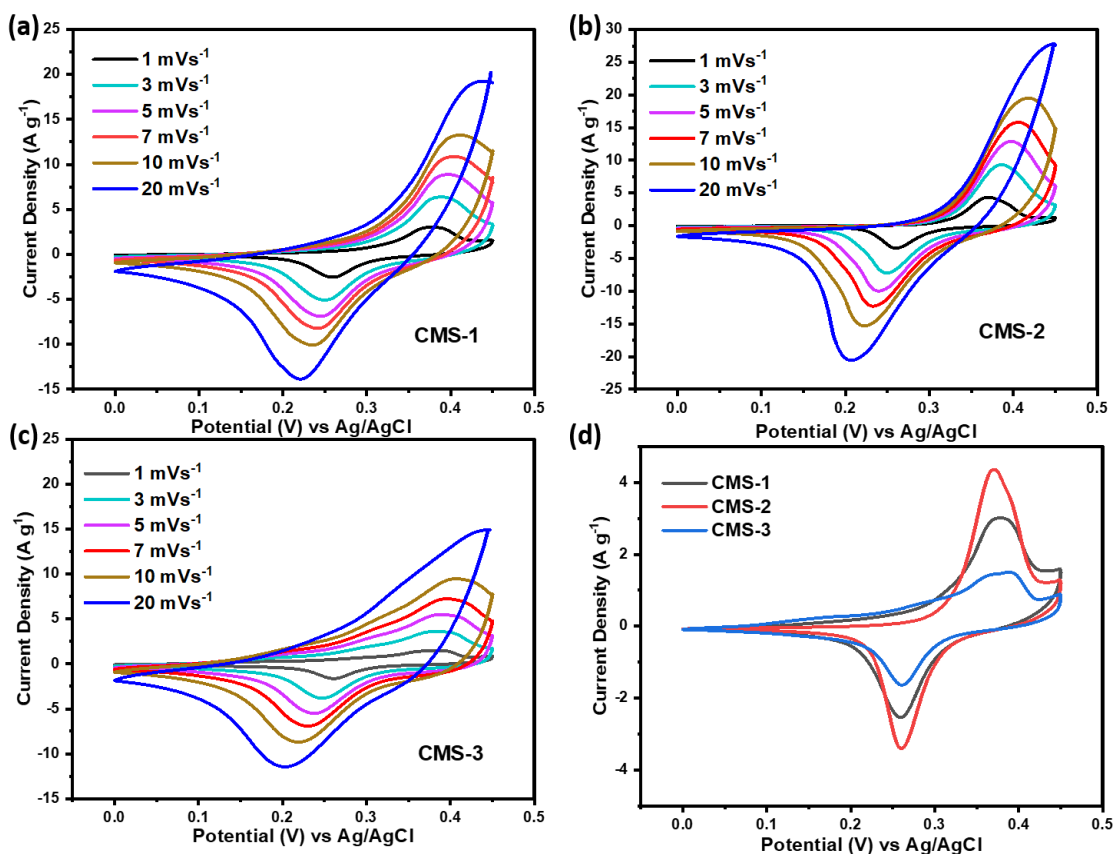
Figure 5.4 CV curve (a) CMS-1 (b) CMS-2 (c) CMS-3 (d) comparison between CMS-1, CMS-2, CMS-3

Increased surface area effects have a significant impact on the pseudo-capacitance of the surface redox process and subsequent intercalation process. Thus, the diffusion-limited process and the redox process need to be enhanced in order to increase the overall storage capacitance of supercapacitors.[34] Fig.7.(a-c) shows the diffusion and capacitive controlled behavior of the three electrodes. Here we can see that the kinetics become more capacitive controlled at high scan rates in all three electrodes. CMS-2 shows less than 20% diffusive behavior at different scan rates which gradually decrease with increase in scan rate making it more capacitive in nature than CMS-1 and CMS-2. Indicating it to be the optimum molar ratio between Mo and Co.

Figure 5.5 The capacity contribution of (a) CMS-1 (b) CMS-2 (c) CMS-3 at different scan rates.

GCD curves of the prepared material is shown in Fig.8. Curve shape is well allined with the hybrid supercapacitor GCD curves. As the current density increses th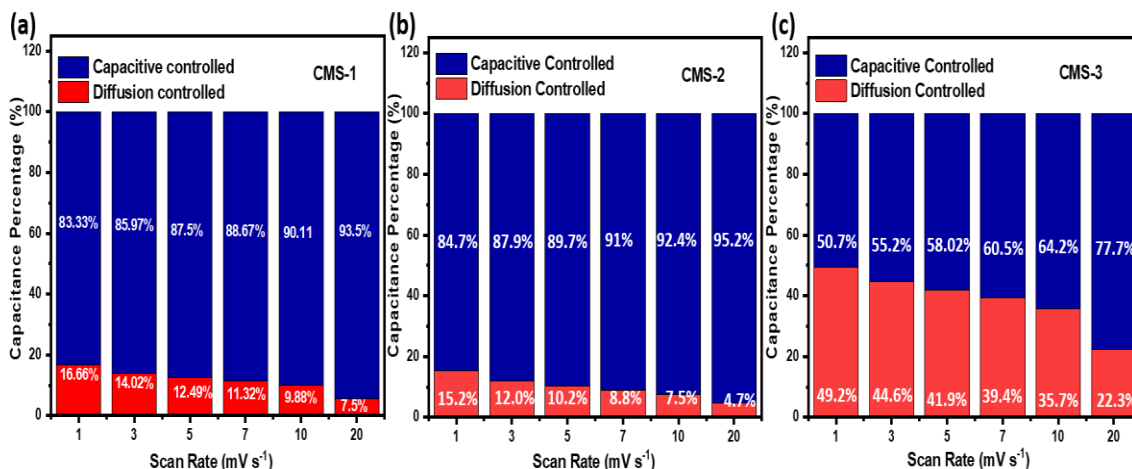e discharge time decreases. All the samples shows maximum discharge time at a current density of 2 A g⁻¹. In GCD curves of CMS-1 and CMS-2 shoulder humps are present indicating the oxidation and reduction peaks present in the CV curve. While in CMS-3 we can see a hump for reduction peak but oxidation peak is not very prominent which is in accordance with its CV curve. As described earlier CMS-3 show a bit inclination towards EDLC behaviour as compared to the other samples. Fig.8.(d) shows the comparison between three samples at 2 A g⁻¹. CMS-2 has the maximum discharge time and hence have the max capacitance which is in accordance with the CV results. The decreases in current with increasing current density is due to the fact as more current will pass per unit time it will take lesss time to discharge while at low current density the current passing per unit time will be less hence resulting in large discharging time. We can see here that the curves are obtained at a current density starting from 2 A g-1 not from 1 A g-1 that is because as we move towards low current density the charging time increases highly it take more time to charge as compared to the discharge time. Although discharge time also incraese but the increase in discharge time is negligible as compared to charging time. For example, when if the charge time increase by 200 to 300 seconds the discharge time increases by 25-30 second only. Foe supercapacitore the charge and discharge time should be equal but at low current densities we see great deviation from idea behaviour so it is recommended to report current densities where we can get and almost ideal behaviour.
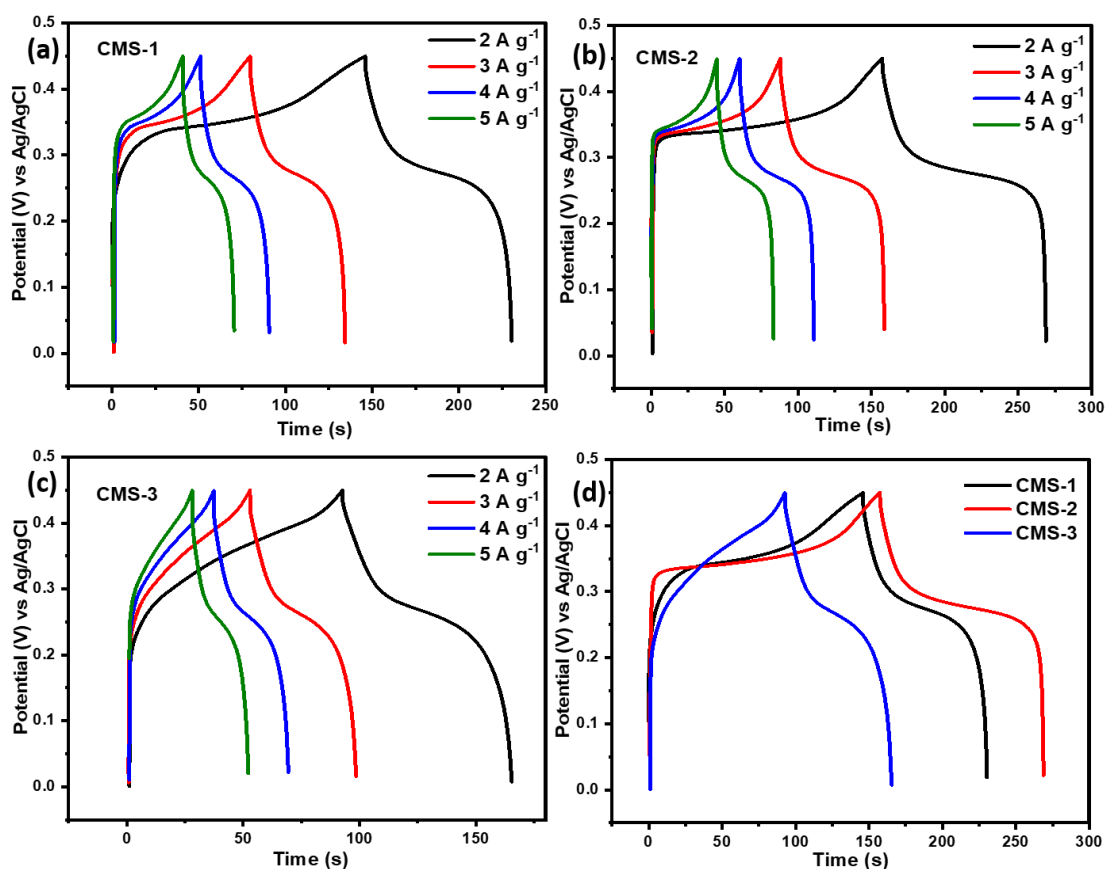
Figure 5.6 GCD graphs of (a) CMS-1, (b) CMS-2, (c) CMS-3 and (d) Comparative graph of three samples

For all three synthesized electrodes, the electrochemical impedance spectroscopy technique was used to investigate electrochemical behaviors, charge transfer resistance, and conductivity over the frequency range of 100 kHz to 1 Hz. The Nequist plot is shown in Fig.9.(a) The linear region of Nyquist plot for CMS-1 and CMS-2 was very close to -Z axis, indicating their excellent conductivity.[40] The semicircle in low frequency region represents the charge transfer resistance. The three electrodes show negligible semicircle which indicate diffused charge transfer resistance in the low frequency region. The slope in high frequency region represent the ionic diffusion. The much steeper slope of CMS-2 in the low frequency region show that it has less ion diffusion resistance and great electron transport efficiency.[41] The resistance value are shown in Table 2

One of the most crucial characteristics of a Supercapacitor is a long cycle life. The electrode needs to be chemically stable for a long time and have a high cyclic capacitance. The electrode with the highest capacitance underwent a stability test by repeating CV measurements for 4000 cycles at a voltage of 100 mV s^{-1}. After 9000 cycles, CMS-2 maintained 92.59% of its capacitance.

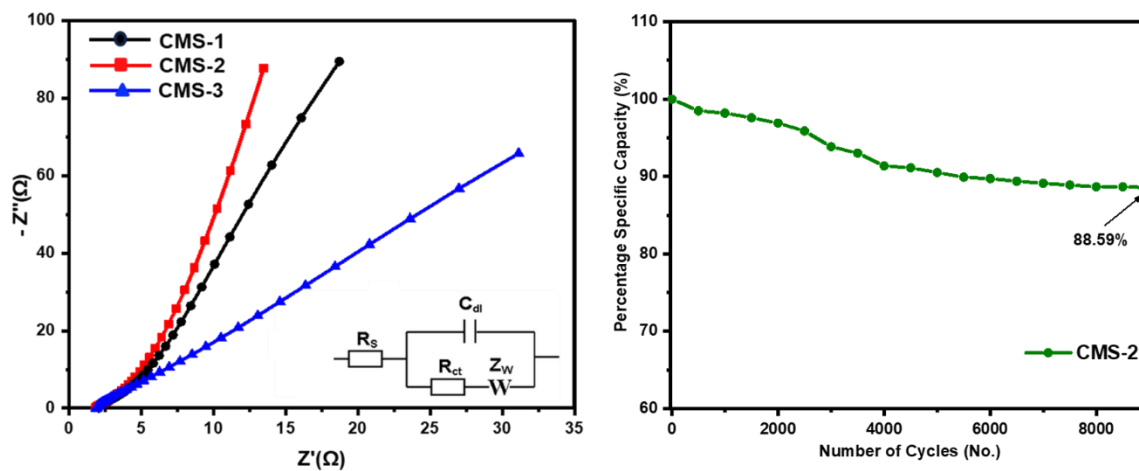**Figure 5.7** (a) Nequist plot of CMS-1, CMS-2, and CMS-3, (b) Cyclic stability graph for 4000 cycles.

Table 2 Charge transfer and solution resistances of CMS-1, CMS-2, and CMS-3

Sample	Specific Capacitance	R_{ct} (Ω)	R_s (Ω)
CMS-1	594 F g^{-1}	0.62	1.82
CMS-2	612 F g^{-1}	0.60	1.80
CMS-3	421 F g^{-1}	0.76	1.87

Table 3 Electro chemical performances of MoS_2 and Co_3S_4 electrodes

Electrode Material	Synthesis Method	Specific Capacitance	Electrolyte	Stability	References
MoS_2/Co_3S_4	Hydrothermal 180 °C for 40 h	612 Fg^{-1}	1M KOH	92% after 4000 cycles	This work
MoS_2	Hydrothermal 180 °C for 40 h	168 Fg^{-1}	1 M KCl	92.6 % after 3000 cycles	[42]
MoS_2	CTAB Assisted Hydrothermal 180 °C for 40 h	160.1 Fg^{-1}	1 M Na_2SO_4	94.8 % after 3000 cycles	[43]
MoS_2	SDBS Assisted Hydrothermal 180° C for 40 h	343 F g^{-1}	1 M Na_2SO_4	120 % after 1000 cycles	[44]
MoS_2	Bath sonication followed by dip coating	395 F g^{-1}	6 M KOH	86 % after 1000 cycles	[45]
$NiCo_2O_4/Co_3S_4$	Hydrothermal at 200 for 12 h	1468 F g^{-1}	3 M KOH	84% after 3000 cycles	[46]
polyhedron-shaped Co_3S_4 nanomaterial	Triethylenediamine-assisted one-step hydrothermal	1038 F g^{-1}	6 M KOH	89.8% after 1000 cycles	[47]

References:

[1] M. Jayalakshmi and K. Balasubramanian, "Simple capacitors to supercapacitors-an overview," *Int. J. Electrochem. Sci,* vol. 3, no. 11, pp. 1196-1217, 2008.

[2] Y. Shao *et al.*, "Design and mechanisms of asymmetric supercapacitors," *Chemical reviews,* vol. 118, no. 18, pp. 9233-9280, 2018.

[3] A. G. Pandolfo and A. F. Hollenkamp, "Carbon properties and their role in supercapacitors," *Journal of power sources,* vol. 157, no. 1, pp. 11-27, 2006.

[4] S. Satpathy, S. Das, and B. K. Bhattacharyya, "How and where to use super-capacitors effectively, an integration of review of past and new characterization works on super-capacitors," *Journal of Energy Storage,* vol. 27, p. 101044, 2020.

[5] M. Lu, *Supercapacitors: materials, systems, and applications*. John Wiley & Sons, 2013.

[6] M. S. Halper and J. C. Ellenbogen, "Supercapacitors: A brief overview," *The MITRE Corporation, McLean, Virginia, USA,* vol. 1, 2006.

[7] Y. Wang, Y. Song, and Y. Xia, "Electrochemical capacitors: mechanism, materials, systems, characterization and applications," *Chemical Society Reviews,* vol. 45, no. 21, pp. 5925-5950, 2016.

[8] S. Cheng *et al.*, "Phase evolution of an alpha MnO2-based electrode for pseudo-capacitors probed by in operando Raman spectroscopy," *Nano Energy,* vol. 9, pp. 161-167, 2014.

[9] P. Simon and Y. Gogotsi, "Materials for electrochemical capacitors," *Nature materials,* vol. 7, no. 11, pp. 845-854, 2008.

[10] M. Salanne *et al.*, "Efficient storage mechanisms for building better supercapacitors," *Nature Energy,* vol. 1, no. 6, pp. 1-10, 2016.

[11] Y. Wang and Y. Xia, "Recent progress in supercapacitors: from materials design to system construction," *Advanced materials,* vol. 25, no. 37, pp. 5336-5342, 2013.

[12] Z. Wu, L. Li, J. m. Yan, and X. b. Zhang, "Materials design and system construction for conventional and new-concept supercapacitors," *Advanced science,* vol. 4, no. 6, p. 1600382, 2017.

[13] Z. Li, J. Lin, B. Li, C. Yu, H. Wang, and Q. Li, "Construction of heteroatom-doped and three-dimensional graphene materials for the applications in supercapacitors: A review," *Journal of energy storage,* vol. 44, p. 103437, 2021.

[14] X. Yu, B. Lu, and Z. Xu, "Super long-life supercapacitors based on the construction of nanohoneycomb-like strongly coupled CoMoO4–3D graphene hybrid electrodes," *Advanced materials,* vol. 26, no. 7, pp. 1044-1051, 2014.

[15] J. F. Snyder, D. J. O'Brien, D. M. Baechle, D. E. Mattson, and E. D. Wetzel, *Structural composite capacitors, supercapacitors, and batteries for US Army Applications*. 2008.

[16] J. Chae, K. Ng, and G. Chen, "Nanostructured materials for the construction of asymmetrical supercapacitors," *Proceedings of the Institution of Mechanical Engineers, Part A: Journal of Power and Energy,* vol. 224, no. 4, pp. 479-503, 2010.

[17] W. Lu, J. Shen, P. Zhang, Y. Zhong, Y. Hu, and X. W. Lou, "Construction of CoO/Co-Cu-S hierarchical tubular heterostructures for hybrid supercapacitors," *Angewandte Chemie,* vol. 131, no. 43, pp. 15587-15593, 2019.

[18] H. Li *et al.*, "Quantifying the volumetric performance metrics of supercapacitors," *Advanced Energy Materials,* vol. 9, no. 21, p. 1900079, 2019.

[19] C. Liu, Q. Li, and K. Wang, "State-of-charge estimation and remaining useful life prediction of supercapacitors," *Renewable and Sustainable Energy Reviews,* vol. 150, p. 111408, 2021.

[20] M. Z. Iqbal, M. M. Faisal, and S. R. Ali, "Integration of supercapacitors and batteries towards high-performance hybrid energy storage devices," *International Journal of Energy Research,* vol. 45, no. 2, pp. 1449-1479, 2021.

[21] A. Allagui, A. S. Elwakil, B. J. Maundy, and T. J. Freeborn, "Spectral capacitance of series and parallel combinations of supercapacitors," *ChemElectroChem,* vol. 3, no. 9, pp. 1429-1436, 2016.

[22] L. Sun *et al.*, "Nitrogen-doped porous graphitic carbon as an excellent electrode material for advanced supercapacitors," *Chemistry–a european journal,* vol. 20, no. 2, pp. 564-574, 2014.

[23] H. Gualous, H. Louahlia-Gualous, R. Gallay, and A. Miraoui, "Supercapacitor thermal modeling and characterization in transient state for industrial applications," *IEEE Transactions on industry applications,* vol. 45, no. 3, pp. 1035-1044, 2009.

[24] Y. Zhan, Y. Guo, J. Zhu, and L. Li, "Power and energy management of grid/PEMFC/battery/supercapacitor hybrid power sources for UPS applications," *International Journal of Electrical Power & Energy Systems,* vol. 67, pp. 598-612, 2015.

[25]   P. Forouzandeh, V. Kumaravel, and S. C. Pillai, "Electrode materials for supercapacitors: a review of recent advances," *Catalysts,* vol. 10, no. 9, p. 969, 2020.

[26]   X. Zhang, F. Zhou, S. Zhang, Y. Liang, and R. Wang, "Engineering MoS2 basal planes for hydrogen evolution via synergistic ruthenium doping and nanocarbon hybridization," *Advanced Science,* vol. 6, no. 10, p. 1900090, 2019.

[27]   L. Zhang *et al.*, "Electrochemical ammonia synthesis via nitrogen reduction reaction on a MoS2 catalyst: theoretical and experimental studies," *Advanced Materials,* vol. 30, no. 28, p. 1800191, 2018.

[28]   A. Ratan, S. Kunchakara, M. Dutt, A. Tripathi, and V. Singh, "Enhanced electrical properties of few layers MoS2-PVA nanocomposite film via homogeneous dispersion and annealing effect induced by 80 MeV Carbon6+ swift heavy ion irradiation," *Materials Science in Semiconductor Processing,* vol. 108, p. 104877, 2020.

[29]   T. Oztas, H. S. Sen, E. Durgun, and B. l. Ortaç, "Synthesis of colloidal 2D/3D MoS2 nanostructures by pulsed laser ablation in an organic liquid environment," *The Journal of Physical Chemistry C,* vol. 118, no. 51, pp. 30120-30126, 2014.

[30]   Z. Li *et al.*, "A facile hydrothemal synthesis of MoS2@ Co3S4 composites based on metal organic framework compounds as a high-efficiency liquid-state solar cell counter electrode," *Journal of Alloys and Compounds,* vol. 831, p. 154910, 2020.

[31]   W. Gu, L. Hu, W. Hong, X. Jia, J. Li, and E. Wang, "Noble-metal-free Co 3 S 4–S/G porous hybrids as an efficient electrocatalyst for oxygen reduction reaction," *Chemical Science,* vol. 7, no. 7, pp. 4167-4173, 2016.

[32]   Y.-R. Liu *et al.*, "Facile one-pot synthesis of CoS2-MoS2/CNTs as efficient electrocatalyst for hydrogen evolution reaction," *Applied Surface Science,* vol. 384, pp. 51-57, 2016.

Chapter 6: Conclusion and Recommendations

6.1 Conclusions

Different molar ratios of Mo and ZIF-67/NPC were analyzed using different characterization techniques and electrochemical testing was performed to check the performance for Supercapacitors. Among the three samples ($Mo_1:Co_{0.5}$, $Mo_1:Co_1$, $Mo_1:Co_2$) the sample with equal molar ratios showed a highest capacitance of 612F g^{-1} than other two samples. The comparatively low specific capacitance in CMS-1 is due to high presence of MoS_2 phase as shown in XRD. From Table 3. It can be seen that generally MoS2 has lower capacitance values and its composite with ZIF-67/NPC showed a positive impact on its specific capacitance due to the formation of Co_3S_4. It reaches a high value in CMS-2 where equal molar mass is present. However, when we increase the molar mass of ZIF-67/NPC to double as compared to Mo a new phase of cobalt sulphides (Co_9S_8) is formed which is less conductive than Co_3S_4 hence decreasing its overall capacitance. Hence CMS-2 is attributed to be the optimum molar mass ratio between Mo and ZIF-67/NPC.

6.2 Recommendations

The electrochemical performance and efficiency of Supercapacitor for energy storage application can be increased by exploring new combination of materials to be employed as electrode, in addition to the informed selection of electrolyte. The following recommendations are presented to address the shortcomings in the research regarding the electrode material for Supercapacitors:

- Focus of the future research should be towards the various transition metals and their oxides in addition to their metal sulphides to be used as efficient material for electrode of Supercapacitors.
- Graphene based material and composites should be explored to enhance the stretch, flexibility and electrochemical performance of the Supercapacitors.
- In contrast to Li-ion batteries, Supercapacitors lack the energy density. Therefore, research is required in the direction of hybrid batteries and Supercapacitors.

- MOFs provide the basis of such application, as they demonstrate large surface area as compared to other compounds and composites. Research should be done to explore the various MOFs compound and their derivatives.

Appendix 1- Publications

Zeolitic imidazolate framework ZIF-67 derived NPC/MoS$_2$ as efficient supercapacitor electrode material

Maryam Raza[1], Naseem Iqbal[1*], Tayyaba Noor[2], Iqra Shauqat, Rabia Ahmad

Abstract:

Here in, we report the synthesis of a ZIF-67-based Molybdenum disulfide composite and analyze the structural and electrochemical properties of the material. A class of zeolitic imidazole framework ZIF-67 (Co) was first synthesized and annealed in a reducing (Ar/H$_2$) environment. The different mass of annealed Co/NPC was added during the hydrothermal preparation of MoS$_2$ to check the effect of Co/NPC while Mo and S amounts were kept constant. Three samples with different mass ratios (Mo$_1$:Co$_{0.5}$, Mo$_1$:Co$_1$, Mo$_1$:Co$_2$) were prepared. XRD analysis confirmed the formation of MoS$_2$/Co$_3$S$_4$ composite. Electrochemical measurement showed a high specific capacitance of 612F g^{-1} of the sample having equal mass ratio of Mo and Co/NPC. The incorporation of Co/NPC significantly improved the electrochemical properties of MoS$_2$. The material also showed a high cyclic stability of 88.59% after 9000 cycles. Among the three samples, the Mo$_1$:Co$_1$ /CMS-2 showed the best performance hence proving to be the optimum ratio.

Keywords: Molybdenum Sulphide, Cobalt Sulphide, Super Capacitor, ZIF-67, Pyrolysis, Specific Capacitance.